CR - 135255

SIGMA
RESEARCH, INC.
2950 GEORGE WASHINGTON WAY
RICHLAND, WASHINGTON 99352

TWO-PHASE WORKING FLUIDS FOR THE TEMPERATURE RANGE 50° TO 350°C

by

ELRIC W. SAASKI

and

PETER C. OWZARSKI

JUNE 1977

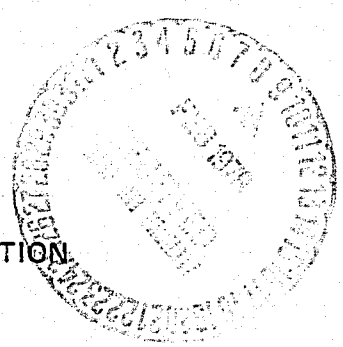

Prepared for

LEWIS RESEARCH CENTER
NATIONAL AERONAUTICS AND SPACE ADMINISTRATION
21000 BROOKPARK ROAD
CLEVELAND, OHIO 44135

1. Report No.	2. Government Accession No.	3. Recipient's Catalog No.
NASA CR-135069		

4. Title and Subtitle	5. Report Date
Two-Phase Working Fluids for the Temperature Range 50° to 350°C	June 1977
	6. Performing Organization Code

7. Author(s)	8. Performing Organization Report No.
Elric W. Saaski and Peter C. Owzarski	None
	10. Work Unit No.

9. Performing Organization Name and Address	11. Contract or Grant No.
Sigma Research, Inc. 2950 George Washington Way Richland, Washington 99352	NAS 3-20222
	13. Type of Report and Period Covered
12. Sponsoring Agency Name and Address	Contractor Report
National Aeronautics and Space Administration Washington, DC 20546	14. Sponsoring Agency Code

15. Supplementary Notes

Final report. Project Manager, Leonard K. Tower, Physical Science Division, NASA Lewis Research Center, Cleveland, Ohio.

16. Abstract

ABSTRACT

The decomposition and corrosion of two-phase heat transfer liquids and metal envelopes have been investigated on the basis of molecular bond strengths and chemical thermodynamics. Potentially stable heat transfer fluids for the temperature range 100°C to 350°C have been identified, and reflux heat pipe tests initiated with 10 fluids and carbon steel and aluminum envelopes to experimentally establish corrosion behavior and noncondensable gas generation rates.

17. Key Words (Suggested by Author(s))	18. Distribution Statement
Heat pipes Materials compatibility Corrosion Decomposition	Unclassified-Unlimited STAR Category 34

19. Security Classif. (of this report)	20. Security Classif. (of this page)	21. No. of Pages	22. Price*
Unclassified	Unclassified	102	

* For sale by the National Technical Information Service, Springfield, Virginia 22161

TABLE OF CONTENTS

LIST OF FIGURES

LIST OF FIGURES (Continued)

LIST OF TABLES

LIST OF TABLES (Continued)

NOMENCLATURE

$(AB),(AB)^+$	chemical species, see Section 2.1.1
B	$\theta \cdot \mathrm{Exp}\left(\frac{3}{8}\theta\right)$
C	total concentration of all stable species, g-mole/cm^3
C_a	concentration of solute species, cm^{-3}
C_a^+	C_a/C_{as}
C_{as}	saturation concentration of solute, cm^{-3}
$[D]$	in Section 2.1, denotes concentration of species D, g-mole/cm^3
D_{ab_+}	diffusion coefficient for solute in solvent, cm^2/sec
D,D^+	chemical species, see Section 2.1.1
E^+	activation energy
E_p	voltage necessary to produce metal and halide gas on inert electrodes at unit concentration, volt
F	Faraday, 23.06 Kcal/volt g-mole
g	gravitational acceleration, cm/sec^2
h_{fg}	heat of vaporization, joules/gm
K_b	solvent thermal conductivity, W/cmK
l	vertical film height, cm
P_ℓ	liquid pressure, dynes/cm^2
P_{vs}	saturated vapor pressure, dynes/cm^2
$Q_{a\ell}$	average heat flux density over $0 \leq z \leq \ell$, W/cm^2
R_1	first-order rate constant, sec^{-1}
R_p	pyrolysis rate constant, sec^{-1}
R_T	total decomposition rate, moles/cm^3 sec
R_{cr}	critical pyrolysis rate for 0.1% decomposition/year, equation (2.2-3)
R_{Fh}	forward reaction rate, high pressure
$R_{F\ell}$	forward reaction rate, low pressure
T_v	vapor temperature, K
T_w	wall temperature, K
$U_{y,z}$	local film velocity in -y and -z directions, cm/sec
y	coordinate perpendicular to wall, cm
z	coordinate parallel to vertical wall, cm

δ	film thickness, cm
ΔE°	electromotive force difference; all reactants at unit concentration, volt
$\Delta E_1, \Delta E_2$	see Figure 2.1-2
ΔG°	free energy change at unit concentrations, Kcal/g-mole
η	similarity variable = y/δ
θ	defined by equation (2.5-13c)
μ_b	solvent viscosity, poise
ν	kinematic liquid viscosity, cm^2/sec
ρ_b	solvent density, g/cm^3
σ	surface tension, dynes/cm

1.0 INTRODUCTION

The efficient transfer of heat in the temperature range 100-350°C has historically been carried out by pressurized liquid loop systems. The heat pipe, however, presents an attractive alternate for both spacecraft and terrestrial applications, due both to its passive operating nature as well as its ability to transfer heat uniformly from complex structures. Delays in the application of heat pipes to this temperature range, however, have come in part from an inability to identify suitable working fluids. Over the past decade, heat pipe development has concentrated on satellite thermal control applications over the temperature range -228° to 100°C. There has also been work done on liquid metal heat pipes for temperatures greater than about 350°C. For applications in the intermediate temperature range of 100 to 350°, there have not been any significant attempts described in the open literature to establish viable fluid/envelope combinations. There has been a limited number of studies up to about 100°C and there has been a continued but generally unsuccessful effort to develop water/metal combinations over the 50 to 350°C range; all common envelope materials, with the exception of copper, generate large amounts of hydrogen gas with water working fluid.

Fluid development in this range is relatively uncharted. Potential space applications include heat transfer components of solar-powered heat engines, thermionic or thermoelectric converters, or high power electronic equipment. In addition, the heat pipe and related two-phase systems are now being increasingly considered for terrestrial uses. Potential applications under active study are in the areas of solar power, geothermal power, and the thermal control of industrial processes.

In solar applications, heat pipes are being considered which must operate from 100-350°C. The lower end of the range is represented by heat pipe heat sinks for solar cells using solar flux concentration and at the upper end by large solar power station designs. In the food processing and other industries, heat pipes are being considered for waste heat reclamation in the range 50° to 300°C while, in the paper industry, two-phase systems are being considered for roll and platen isothermalization.

The work summarized here was an initial analytical and experimental investigation into suitable working fluids for the range 100 to 350°C. Because the number of potential working fluids is almost unlimited, basic differences in chemical structure and bonding were used to categorize and rank large groups of compounds with similar chemical and stability characteristics. From this ranking, 10 fluids were selected for long-term reflux compatibility tests in aluminum and mild steel envelopes. The fluids selected were not necessarily the most stable compounds, but rather represented distinct chemical groups of interest. These groups were

1. Aliphatic hydrocarbons
2. Aromatic hydrocarbons
3. Halogenated hydrocarbons
4. Inorganic molecular fluids.

2.0 ANALYSIS AND BACKGROUND

Theoretical models for decomposition of organic molecules will be discussed in Section 2.1 and, in Section 2.2, this basis will be used for analysis of known data and prediction of organic species stability.

2.1 Thermal Decomposition

Working fluids for high temperature operation must be stable relative to several different modes of chemical reaction. All molecules, however, will ultimately break up into lower molecular weight molecules, radicals and/or constituent atoms at high temperatures. This behavior is termed pyrolysis and is of primary importance.

Pyrolysis is the ultimate mode of working fluid failure at high temperature. Fortunately, a great deal of work has been done on gas phase pyrolysis and this information is invaluable in defining potentially stable high temperature working fluids.

2.1.1 Physical Models for Pyrolysis

In one of the most useful physical models of pyrolysis, all bonds within a molecule are assumed vibrating at some characteristic quantum mechanical frequency, with each bond alternately being compressed and stretched relative to the equilibrium bond length. In the model of Rice, Ramsperger and Kassel[1] (RRK), the various oscillating bonds are mechanically coupled so that there exists a finite probability that enough energy will be transferred to a single bond to break it and thereby destroy the molecule. This critical energy is called the activation energy. Using either statistical mechanic methods or classical mechanical models, the first-order rate of bond breakage is given as

$$R_1 = A \cdot EXP\ (E^+/RT) \qquad (sec^{-1}) \qquad (2.1\text{-}1)$$

where E^+ is the activation energy and A is a constant. This rate equation is of the Arrhenius form, with an exponential energy term and a pre-exponential multiplier. The constant A from RRK theory is in the range 10^{12} to 10^{14} sec^{-1}, and is of the same order as the bond vibrational frequencies.

Although the thermal decomposition of a gas is obviously closely associated with the rate of bond breakage, it is not always correct to assume that the rate of gas decomposition is exactly equal to the bond breakage rate. At high pressures, for example, an activated molecule that possesses a bond energy greater than the critical value E^+ may not decompose if collisions with lower energy molecules deactivate it. This possible complexity of pyrolysis is best illustrated by considering a hypothetical species "D" that yields decomposition products A and B, that is,

$$D \rightleftarrows A + B \qquad (2.1\text{-}2)$$

Complexity arises because the pyrolysis reaction may actually involve many intermediate reactions and activated species. These species can be conveniently defined relative to the amount of energy needed to form D from A and B, and to the energy required to decompose D into its constituents, A and B. These energies and the possible intermediate species are combined in the potential energy profile of Figure 2.1-1. In this figure, bond internal energy is plotted versus a "reaction coordinate", which can be considered proportional to bond length. The energy of formation for D is shown as ΔE_2, and the decomposition energy as E^+, or the sum of ΔE_1, and ΔE_2.

In addition to the species A, B, and D, this figure shows five other intermediate species:

i) D^+ corresponds to molecules of D that have an internal energy $>E^+$

ii) $(AB)^+$ corresponds to molecules of AB that have an internal energy adequate to form D^+

iii) (AB) corresponds to an intermediate combination of A and B that cannot directly form D^+

iv) A^+ and B^+ correspond to activated forms of A and B having adequate energy to directly form $(AB)^+$.

At any point in time, these species are in quasi-equilibrium, as illustated by the various rate constants of Figure 2.1-2. Since each of the species combinations shown in Figure 2.1-2 is coupled to other species by both forward and reverse rate constants (K_i), a total of 16 rate constants must be determined

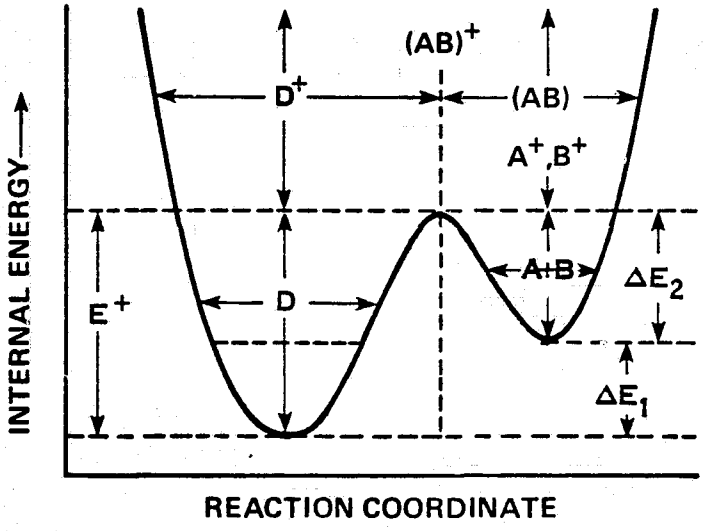

FIGURE 2.1-1. VARIOUS SPECIES OF POTENTIAL IMPORTANCE IN THE THERMAL DECOMPOSITION REACTION $D \rightleftharpoons A+B$

7706-232.3

FIGURE 2.1-2. UNIMOLECULAR DECOMPOSITION OF SPECIES D TO A+B

7706-232.4

to fully characterize the pyrolysis reaction. Under certain conditions, however, the pyrolysis rate is considerably simplified as, for example, when the concentration of A and B is low or when E^+ is much greater than ΔE_2. In the following section, various cases such as these will be considered.

2.1.2 Rate Equations for D $\rightleftarrows$ A + B

As presented in Reference (1), the rate R_f for loss of D by pyrolysis is approximately

$$R_f \cong [D] \left(\frac{K_1}{K_2}\right) K_3 \cdot \frac{1}{1 + K_3/CK_2} \qquad \text{(g-moles/cm}^3 \text{ sec)} \quad (2.1\text{-}3)$$

where C is total concentration. This form is derived assuming the energy ΔE_2 to form $(AB)^+$ from (AB) is greater than zero, that $K_7 >> PK_6$, and that the concentration of D is much greater than A or B (as in the early stages of pyrolysis). Under these conditions, it can be seen that the intermediate species concentrations do not influence the decomposition rate, but that the decomposition rate is dependent on system pressure. This pressure dependence appears because molecular collisions activate as well as deactivate the species D; the rate constants K_1, K_2, K_5, and K_6 have as units 1/sec atm. At low pressure, the loss rate will be

$$R_{f\ell} \cong C[D]\, K_1 \qquad \text{(g-moles/cm}^3 \text{ sec)} \quad (2.1\text{-}4)$$

Since A and B are in small concentration, the concentration C is proportional to the concentration of D, and the pyrolysis rate increases as $[D]^2$. At high pressure, the rate will be

$$R_{fh} \cong [D]\left(\frac{K_1}{K_2}\right) K_3 \qquad (2.1\text{-}5)$$

If it is assumed that the energy ΔE_2 to form $(AB)^+$ from (AB) is very close to zero, as in the case that A and B are free radicals, then the low and high pressure rates are

$$R_{f\ell} \cong C[D]\, K_1 \qquad \text{(low pressure)} \quad (2.1\text{-}6)$$

and

$$R_{fh} \cong \frac{[D]}{2}\left(\frac{K_1}{K_2}\right) K_3 \qquad \text{(high pressure)} \qquad (2.1\text{-}7)$$

Hence, if the activation energy for decomposition is measured at low pressure and high pressure, there conceivably will result two differing values, of which only the high pressure value will be independent of pressure. Physically, this behavior is due to the fact that at low pressure, virtually every molecule that achieves the activated state D^+ will decompose before a collision occurs with another molecule, while at high pressure, deactivating collisions represented by CK_2 become important. Table 2.1-1 from Benson[1] presents approximate values of pressure at which the decomposition rate shows a factor of two reduction from the high pressure limit. Because of the energy-absorbing effects of multiple bonds, the high pressure limit falls as the number of atoms (and internal degrees of freedom) within a molecule increases. The values presented should be considered to have an uncertainty of about a factor of 10.

TABLE 2.1-1. APPROXIMATE PRESSURE AT WHICH UNIMOLECULAR RATE CONSTANTS FALL FROM THE HIGH PRESSURE LIMIT BY A FACTOR OF TWO

Number of Atoms in Molecule	Degrees of Freedom	Characteristic Pressure (atm, STP)
2	1	4000.
2	2	225.
3	3	25.
3	4	4.
3	5	1.
4	6	0.3
4	7	0.09
4	8	0.03
5	9	0.01
5	10	0.005
5	11	0.003
6	12	1.2E-3

As an example of the pressure-dependence of rate constants, Ingold, et al present thermal decomposition data for several normal paraffin hydrocarbons.[2] For propane, butane, and pentane, a low pressure (0.0-0.66 atm) rate equation of the form

$$R_{F\ell} \cong AP + BP^2 \qquad (\text{moles/cm}^3\ \text{sec}) \qquad (2.1\text{-}8)$$

was found, while at high pressure (>0.66 atm) a linear relationship was indicated,

$$R_{Fh} \cong A'P \qquad (\text{moles/cm}^3\ \text{sec}) \qquad (2.1\text{-}9)$$

where A', A, and B are curve-fitting rate constants, and P is pressure. At both high and low pressure, the rate constants were exponential in temperature in accordance with models discussed in Section 2.1.1, but differed considerably in value, as shown in Table 2.1-2.

TABLE 2.1-2. EFFECT OF PRESSURE ON THE ACTIVATION ENERGY E^+ (Kcal/g-mole) FOR DECOMPOSITION OF NORMAL HYDROCARBONS(1)

Method of Calculation	n-propane	n-butane	n-pentane	n-heptane
Extrapolation to zero pressure	71	75	93	88
Extrapolation to infinite pressure	68	59	63	59

(1) From Ingold et al.[2] Energy E^+ is Kcal/g-mole.

As an example of decomposition being rate-limited by free radical production, in the pyrolysis of toluene at a constant pressure of 0.008 atm and temperatures between 738 and 964°C, Szwarc obtained a reaction product gas which was essentially 40% methane and 60% hydrogen. The gases were also accompanied by dibenzyl in the ratio of 1 mole per mole of gases. The rate constant was exponential in temperature and corresponded to an activation energy of 77.5 Kcal/mole.[3] Later measurements by Price indicate a more accurate value of 85 Kcal/mole.[4] Because of the products formed, the decomposition mechanism was attributed to be rate-limited by production of benzyl and hydrogen free radicals

$$\phi CH_3 \rightleftharpoons \phi CH_2\cdot + H\cdot \qquad (2.1\text{-}10)$$

and the 77.5 Kcal/mole is equivalent to activation energy E^+ in Figure 2.1-1. For free radicals, $E_2 \approx 0$, so that equations (2.1-6) and (2.1-7) are appropriate for description of the reaction rate. The energy E^+ is the bond dissociation energy for free radical production. This important quantity is discussed in more detail in Section 2.2.

In summary, the thermal decomposition of a gaseous species is generally characterized by

1. an Arrhenius-type of rate equation with a pre-exponential factor $\sim 10^{13}$ sec^{-1};
2. a concentration-dependent rate constant at low pressure;
3. a relatively concentration-independent rate constant at high pressure.

These conclusions hold for many simple systems, but there are some exceptions to these generalizations and care must be exercised in their use.

2.2 Definition of Stable Organic Species

A stable molecule is obviously one in which the various intramolecular bonds have high stability, and bond stability is the basic factor determined in pyrolysis experiments. A large body of data exists on both the pyrolysis of organic compounds to form stable molecules and the pyrolysis of organic

compounds to form free radicals. These data can be of significant help in defining high temperature two-phase working fluids, particularly if the data are interpreted on the basis of bond strength.

In the previous section, the mechanisms associated with pyrolysis were described. A critical bond dissociation energy E^+ was invoked, but no attempt was made to characterize and define bond strength in terms of organic structure. That is, the number of possible organic compounds is infinite for all practical purposes and pyrolysis data are available for only a very small number of these compounds. However, the physical structures of many organic molecules are closely related, and examination of bond strengths for groups of homologous compounds is possible and practical. In addition, covalent electron pair bonds retain much of their identity regardless of what is occurring in the remainder of the molecule, and hence bond dissociation energies can often be used even with considerable change elsewhere in the molecule.

2.2.1 Bond Theory of Stable Molecules

Chemical bonding in organic molecules is chiefly covalent and dominated by the formation of hybrid electron orbitals. Although accurate quantum mechanical representations for compounds of carbon cannot be calculated, it is possible to show that certain linear combinations of the standard s, p, and d electronic orbitals possess minimum energy and, hence, high stability.

One type of hybrid orbital is designated "sp", and is formed by combining an s orbital with a p orbital to form two equivalent sp orbitals. The orbitals are oriented 180^o from each other. In the sp^2 hybridization, a single s orbital and two p orbitals form three equivalent hybrid sp^2 orbitals, on a 3-cornered arrangement. The sp^3 hybrid is formed from one s orbital and three p orbitals and is tetrahedral.

Because of their greater s character, sp orbitals are generally smaller than sp^2 orbitals and sp^2 orbitals are smaller than sp^3 orbitals. A small orbital generally indicates a short, strong bond, and bond strength increases as $sp^3 < sp^2 < sp$. The hybrid orbitals are highly localized and individually cylindrically symmetric. The cylindrically symmetric covalent bonds formed by these orbitals are commonly called σ bonds.

In some chemical combinations, the hybrid bonds do not accommodate all available electrons and additional electrons are available in the remaining lobar p orbitals. If the p orbitals of the adjacent atoms overlap, then a hydrid orbital of "π electrons" is formed. The π electron clouds reduce the energy of the molecule even further and, hence, indicate a high bond strength.

An example of sp hybridization is acetylene, C_2H_2, which has a triple bond between carbons, and hydrogen bonds formed from sp hybrids. Remaining electrons are found in a delocalized π cloud formed from the initial p orbitals. Because of the short sp bond length and π cloud, the acetylene molecule is very stable towards thermal bond breaking.

An example of sp^2 hybridization is ethylene, C_2H_4, which is a combination of two sp^2 orbitals and a delocalized π electron cloud. Because of the relatively short sp^2 bonds and the contributing π bonds, ethylene is also quite stable, although less so than acetylene. A particularly stable species is the ring compound benzene, which is composed of localized sp^2 bonds and a π cloud above and below the ring. All aromatic compounds (benzene ring type) exhibit this bonding and the rings are highly stable.

Examples of sp^3 hybridization are found at each carbon atom in the saturated paraffins, methane, ethane, propane, etc. No π bonds are formed.

2.2.2 Predicting Stability on the Basis of Chemical Structure

To paraphrase the discussion in Section 2.2.1, the thermal stability of organic vapors is in large part determined by the individual bond strengths of highly localized hybrid orbitals (σ bonds) and delocalized hybrid orbitals (π bonds). It is furthermore an experimental fact that substitutions at non-carbon σ bond positions do not significantly influence the stability of other σ bonds on a carbon skeleton, so that the search for highly stable classes of organic compounds can be performed by

1. characterizing the bond dissociation energies of various σ bonds, and particularly C-H bonds;
2. defining classes of compounds with π orbital bonding;
3. correlating 1 and 2 above with available data in the literature.

Bond dissociation energies for free radical production are presented in Table 2.2-1 for a large number of organic compounds. Dissociation energies range from a low of about 40 Kcal/mole to a high of about 120 Kcal/mole. Since most organics will have some C-H bonds, it is necessary to define classes of compounds that have a strong C-H bond; as in the case of toluene discussed earlier, the splitting off of H• is often a primary decomposition mode. As discussed in the previous section, acetylene and ethylene are seen to have strong bonds for C-H coupling, but unfortunately are not suitable for high temperature use because of high vapor pressures and low critical temperatures.

TABLE 2.2-1. BOND DISSOCIATION ENERGIES FOR VARIOUS WORKING FLUID VAPORS (Kcal/mole)[1]

	H	CH_3	C_2H_5	CHO	OH	F	Cl	Br	I	NH_2	CN	C_2H
H	104	104	98	~79	119	136	103	88	71	104	120	
CH_3	104	88	85	71-75	88	108	84	70	56	79	105-110	
C_2H	<121	~110	~109									
C_2H_3	104	92	~90	~84			84		~55		~121	
CH_3CO	89	81	83	~59	110	119	79	~67	~51	~98		
C_2H_5	98	85	85	~71	90		81	69	53	78		
C_2H_5O	102	80	82		42	–	–	–	–			
n-C_3H_7	98	85	79	~71			82	69	50	77		~106
i-C_3H_7	95	84	~75		92	106	81	68	53	85		~103
n-C_4H_9	94	78	78									
t-C_4H_9	91	80			91		79	63	50	84		
C_6H_5	112	93	94	~83	96	125	86	70-72	61	~94	~124	~119
$C_6H_5CH_2$	85	70	68		77		68	51	38	59	~95	
$C_{10}H_7$								70				
$C_{10}H_7$-CH_2	~76											

1) Variations of ± 10 Kcal/mole are not uncommon among different investigators.

Because of the π bonding and sp^2 hybridization of benzene (C_6H_6) and napthalene ($C_{10}H_8$), both have excellent C-H bond strengths, and are candidate working fluids. Benzene, unfortunately, has a rather low boiling point of 80.1°C, but the boiling point of napthalene is 218°C and is attractive on this basis as well. Its melting point is 80.55°C.

A number of other aromatic organic fluids may also be of interest on the basis of bond dissociation energies, including toluene and fluoro- and chloro-substituted benzene compounds. The well-known Dowtherm working fluids are also aromatics. Dowtherm E is O-dichlorobenzene, and Dowtherm A is 26.5% diphenyl (C_6H_5-C_6H_5) and 73.5% diphenyl oxide (ether) (C_6H_5-O-C_6H_5). Dowtherm E may split off HCl, and Dowtherm A may split off a water molecule on decomposition, and their performance in heat pipes has not been totally satisfactory in the author's previous experience and in use by others.[5] It is not clear whether the decomposition seen results from impurities or from the fluids themselves. This is discussed later in this report.

2.2.3 Related Literature

Tables 2.2-2 and 2.2-3 present experimental rate constants for the thermal decomposition of a number of organic molecules. The data presented in these tables reflect the formation of the "first" product of pyrolysis. In the case of obvious stable compounds (Table 2.2-2), compounds or radicals have not been identified. In the case of free radical formation (Table 2.2-3), the free radicals eventually react to form secondary permanent compounds. For instance, toluene pyrolysis proceeds through the free radical ϕ-CH_2- and H but eventually H_2, CH_4 and $\phi CH_2CH_2\phi$ are observed products. In any case, the chemical nature of the heat transfer fluid has been altered, and mechanism and products are of lessor importance.

The pyrolysis rate constants in Tables 2.2-2 and 2.2-3 are of the Arrhenius form

$$R_p = A \cdot EXP\ (-E^+/RT), \qquad (sec^{-1}) \qquad (2.2\text{-}1)$$

and the value of R_p at 350°C is tabulated in the tables. If the decomposition of vapor D is given as

$$\frac{dD}{dt} = -DR_p \qquad (moles/sec) \qquad (2.2\text{-}2)$$

TABLE 2.2-2

EXPERIMENTAL GAS-PHASE RATE CONSTANTS FOR PYROLYSIS REACTIONS THAT TERMINATE WITH STABLE MOLECULES

Reactant	Product	Log A, sec^{-1}	E^+, Kcal/mole	r_{350}, hr^{-1}	Ref.
CH_2F_2	---	12.95	70.2	7.6E-9	6
CHF_3 (R-23)	---	13.44	69.0	6.2E-8	6
CF_2HCl (R-22)	C_2F_4+HCl	12.36/13.84	51.4/55.8	7.7E-3/6.7E-3	7, 8
$CClF_2$-$CClF_2$ (R-114)	---	---	---	~1.8E-6	9
$CClF_2$-CF_2-$CClF_2$ (R-116)	---	---	---	~1.4E-6	9
CF_2Cl_2 (R-12)	---	12.5	67.0	3.6E-8	10
CH_4	---	12.0	79.4	5.1E-13	11
C_2H_6	---	16.06/14.1	77.7/69.8	2.3E-8/1.5E-7	11
C_3H_8	---	13.44/16.6	62.1/74.9	1.6E-5/7.7E-7	11
n-C_4H_{10}	---	12.71/13.53	57.7/61.4	4.8E-5/3.5E-5	11
i-C_4H_{10}	---	13.92	63.5	1.6E-5	12
n-C_5H_{12}	---	13.4	61.2	3.1E-5	11
n-C_6H_{14}	---	12.43/14.58	55.5/64.5	3.3E-4/3.3E-5	11
Toluene	H_2, CH_4	13.3/14.8	77.5/85	4.7E-11/3.5E-12	13, 14
Benzene					
Napthalene					

TABLE 2.2-2 (Continued)

EXPERIMENTAL GAS-PHASE RATE CONSTANTS FOR PYROLYSIS REACTIONS THAT TERMINATE WITH STABLE MOLECULES

Reactant	Products	Log A, sec^{-1}	E^{+}, Kcal/mole	r_{350}, hr^{-1}	Ref.
Perfluoro-cyclobutane	C_2F_4	15.95	74.1	3.3E-7	13
t-butyl alcohol	Isobutene + H_2O	14.68	65.5	1.8E-5	
Cyclobutane	C_2H_4	15.6	62.5	1.7E-3	
Vinylcyclohexene-3	Butadiene	15.7	61.8	3.8E-3	
CH_3CH_2Cl	C_2H_4 + HCl	14.6	60.8	6.8E-4	
t-Amyl alcohol	Pentenes + H_2O	13.51	60.0	1.1E-4	
Cyclopentene	Cyclopentadiene + H_2	13.04	58.8	9.4E-5	
Cyclohexene	C_2H_4 + Butadiene	12.9	57.5	1.9E-4	
n-butylchloride	Butane-1 + HCl	14.0	57.0	3.7E-3	
$CH_3CH_2CH_2Cl$	$CH_3CH = CH_2$ + HCl	13.45	55.0	5.2E-3	
$CH_3CHClCH_2Cl$	$CH_3CH = CHCl$ + HCl	13.8	54.9	1.3E-2	
Acetyl cyclobutane	C_2H_4 + $CH_3COCH = CH_2$	14.53	54.5	9.4E-2	
CH_3CH_2Br	C_2H_4 + HBr	12.86	52.3	1.2E-2	
n-butyl bromide	Butene-1 + HBr	13.18	50.9	7.6E-2	
$CH_3CHBrCH_3$	$CH_3CH = CH_2$ + HBr	13.00	50.7	5.9E-2	
$CH_3CHClCH_3$	$CH_3CH = CH_2$ + HCl	13.4	50.5	0.175	
Isobutyl bromide	Isobutene + HBr	13.05	50.4	8.5E-2	
CH_3CHCl_2	$CH_2 = CHCl$ + HCl	12.1	49.5	2.0E-2	

TABLE 2.2-3

EXPERIMENTAL GAS-PHASE PYROLYSIS RATES FOR PRODUCTION OF FREE RADICALS[1]

Reactants	Products	Log A, sec^{-1}	E^+, Kcal/mole	R_p @ 350^o, hr^{-1}
ϕCH_3	$\phi CH_2 + H$	12.32/14.8	77.5/85	4.9E-12/3.5E-12
$m\text{-}CH_3\text{-}\phi\text{-}CH_3$	$CH_3\text{-}\phi\text{-}CH_2 + H$	12.62	77.5	9.9E-12
$p\text{-}CH_3\text{-}\phi\text{-}CH_3$	$CH_3\text{-}\phi\text{-}CH_2 + H$	12.68	76.0	3.8E-11
$O\text{-}CH_3\text{-}\phi\text{-}CH_3$	$CH_3\text{-}\phi\text{-}CH_2 + H$	12.68	75.0	8.5E-11
α, β-Me-Napthalene	α,β-Me-Napthyl + H	13.18	73.5	9.0E-10
ϕ_2CH_2	$\phi CH + H$	13.0	73.0	9.0E-10
ϕBr	$\phi + Br$	13.3	70.9	9.7E-9
$\phi\text{-}CH_2\text{-}CH_3$	$\phi CH_2 + CH_3$	13.0	63.0	2.9E-6
$\phi CH_2\text{-}COCH_3$	$\phi CH_2 + COCH_3$	13.9	63.0	2.3E-5
$CH_3COCOCH_3$	$2CH_3CO$	13.8	60.0	2.1E-4
$\phi CH_2\text{-}NH_2$	$\phi CH_2 + NH_2$	12.8	59.0	4.6E-5
$\phi CH_2\text{-}C_2H_5$	$\phi CH_2 + C_2H_5$	13.5	57.5	7.7E-4
$CH_3\text{-}NO_2$	$CH_3 + NO_2$	13.6	50.6	0.256
$\phi CH_2\text{-}Br$	$\phi CH_2 + Br$	13.0	50.5	0.07

(1) Data primarily from Ref. 1.

then for a hypothetical maximum allowable 0.1% decomposition of the initial fluid in 1 year, the critical value of R is

$$R_{cr} = 1.14\ (10^{-7})\ hr^{-1} \qquad (0.1\%/yr) \qquad (2.2\text{-}3)$$

On review of the various values of R_p in Tables 2.2-2 and 2.2-3, it can be seen that the halogenated hydrocarbons are marginal on this basis ($R_p > R_{cr}$), and that no paraffinic hydrocarbons have both a low decomposition rate and a reasonable vapor pressure at 350°C. Iso-butane, for example, has a rate constant of 1.6E-5 at 350°C, and a boiling point of -12°C. Other higher molecular weight and lower pressure paraffins have higher decomposition rates.

Both toluene and methyl-napthalene have dissociation rates on the order of 1.E-9 or less, and illustrate the superior high temperature properties of the aromatics.

One of the most serious results of the pyrolysis of a two-phase heat transfer fluid is the production of low boiling point secondary compounds, or non-condensable gases (NCG). These gases, typically hydrogen in the case of organics, inhibit condensation heat transfer. By itself, the pyrolysis data above are useful but not complete in that there is still uncertainty in the rate of NCG production since the pyrolysis may not terminate with a gaseous product. Figure 2.2-1 shows the formation rate of NCG by pyrolysis for eight fairly stable organic working fluids as a function of temperature in the Arrhenius fashion (1/T). Since Table 2.2-3 showed that the most stable fluids had activation energies (E*) in the region around 70 Kcal/mole, the above figure shows a performance uncertainty band around this value. Fluids behaving within the band can be considered as suitable for heat pipe use below about 400°C, depending on longevity requirements.

Seifert et al.

Some pertinent work on high temperature stability of heat transfer fluids was carried out by Seifert, Jackson, and Sech.[17] Their interest was in liquid phase stability of 24 compounds or mixtures in the temperature range of

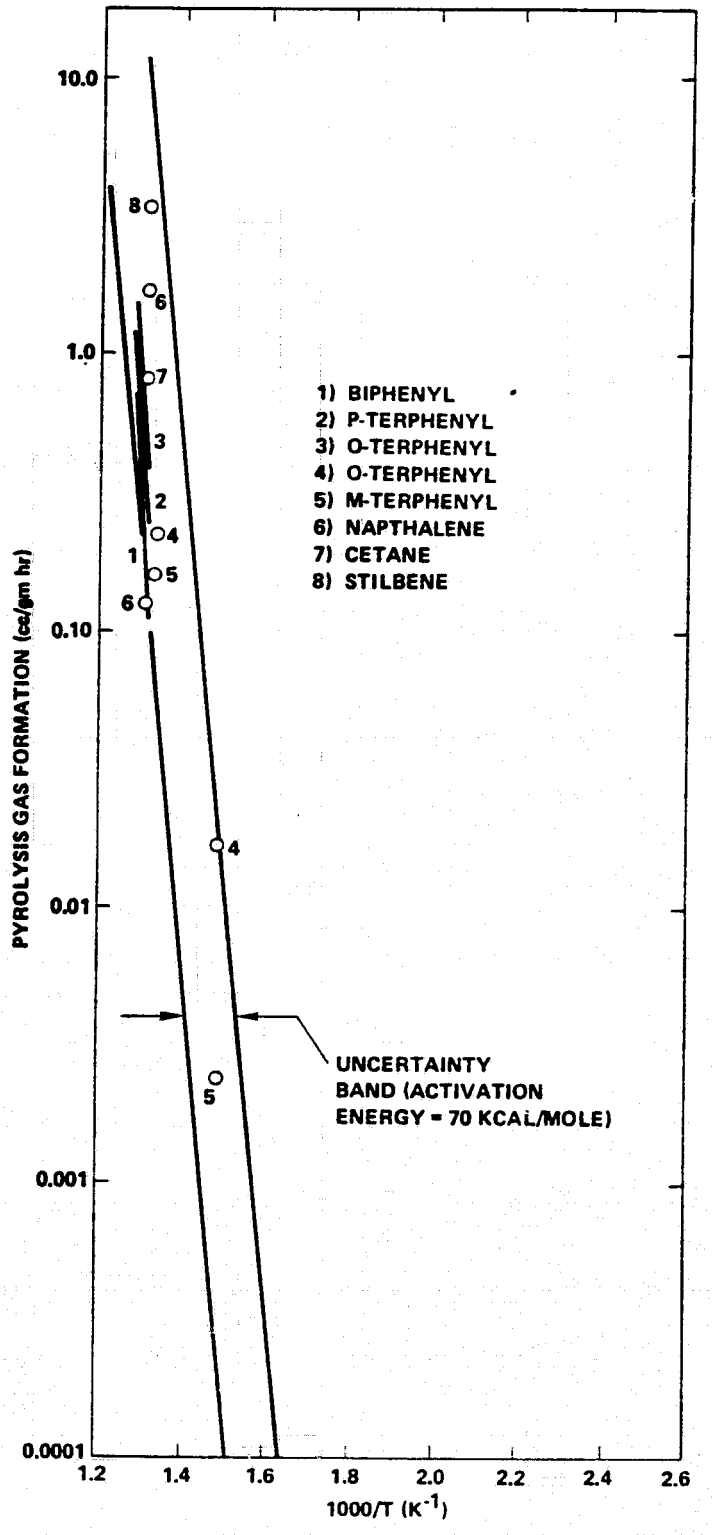

FIGURE 2.2-1. PYROLYSIS DATA FOR VARIOUS POLYPHENYL AND ORGANIC WORKING FLUIDS (REF. 15 AND 16)

7706-232.2

343-413°C (650-775°F). Samples were heated in stainless steel tubes containing O_2 free nitrogen. After testing, percent weight loss, presence of residual pressure (at -70°C), and physical state were noted before the fluid was analyzed by gas chromatography. Analyses were reported as low boiling products, original fluid and high boiling products. Results from 16 organic fluids (8 other halogen organic fluids are discussed later) are summarized in Table 2.2-4. Quantitative pyrolytic damage is only indicated by percent original material lost, or percent higher and lower boiling fractions. Qualitative damage is indicated by physical state, color and presence of NCG. The lower boiling fractions would probably appear as noncondensable gas in a heat pipe or other two-phase heat transfer device.

The most significant observations to be made are the high stability of the aromatic ethers and the variable stability of alkylated aromatic ethers. For the latter, dealkylation seems to be the primary form of pyrolysis, with ortho substituted alkyl groups being least stable.

Miller et al.

Another search for high temperature working fluids, this time for Automotive Rankine engines, provides a somewhat qualitative set of results for apparent vapor phase pyrolysis of organic working fluids. One hundred ten fluids were studied by heating small quantities to 382°C (720°F) in carbon steel containers without removing atmospheric air. Minimum test times were 24 hours and decomposition was ascertained by visual inspection (color, solids content) and/or presence of strong acid. Of the 110, eleven organic fluids not containing halogens passed the minimum 24-hour test and nine (nonhalogen) organic-water mixtures were tested at the same temperature. The results are summarized in Tables 2.2-5 and 2.2-6. At the elevated temperature (382°C) all the specimens were in the gas phase since the critical temperature was exceeded. Even the water-fluid mixtures were vaporized (T_o = 374°C for water). With the small amount of air present, some oxidative degradation was likely. Most organic compounds readily oxidize in contact with liquid water and air under pressure at about 250°C and higher.[18] This could have been a mode

TABLE 2.2-4

STATIC THERMAL STABILITY COMPARISONS OF SELECTED ORGANIC FLUIDS

Compound (freezing point and normal boiling point, °C)	Length of Test (weeks)	Temp. (°C)	Sample Lost-%	Physical[a*] State	Gas Chromatographic Analysis: Color	Residual[b*] Pressure	Weeks at °C	% Lights[d*] (L)	% Higher[e*] (H)	Σ % L+H
Diphenyl ether - diphenyl eutectic (12.2, 257)	0	-	-	L	Lt.Yellow	--	2,413			9.5
	3	413	1.9	L	Yellow	No	4,413			5.5
	2	413								
	4	413								
Biphenylyl phenyl ether (isomer mixture) (37.2, 360)	0	-	-	S	White	--				
	4	343	2.1	VL	Brown	No				
	6	399	5.7	VL	Black	No				
	2	413	3.1	VL	Brown	No	2,413			4.9
	4	413	2.6	VL	Brown	No	2,413			11.9
o-biphenylyl phenyl ether (50, 354)	0	-	-	S	White	--				
	3	399	1.0	VL	Tan	No	2,413			4.5
	4	413	1.3	VL	Brown	No	4,413			10.4
m-biphenylyl phenyl ether (not available)	0	-	-	L	Yellow	--				
	2	413	2.5	L	Brown	No				
	4	413	2.3	L	Brown	No				
di- and triaryl ethers[2*] (<-18, 300)	0	-	-	L	Yellow	--				
	8	343	2-4[c]	L	Brown	No	4,343			0.3
	4	371	2-4[c]	L	Brown	No	4,385			4.4
	3	399	2-4[c]	L	Brown	No	1,413	0.7	5.1	5.8
	3	413	2-4[c]	L	Brown	No	4,413	2.4	7.0	9.4
Dimethyl diphenyl ether[3*] (isomer mixture) (-40 pour point, 290)	0	-	-	L	Colorless	--				
	4	343	3.2	L	Brown	No				
	3	371	17	L	Black	Yes				
	3	399	24	VL	Black	Yes				
Tetramethyl diphenyl ether (isomer mixture) (N.A., 310)	0	-	-	L	Yellow	--				
	2	343	1.5	L	Yellow	No				
	4	343	1.7	L	Brown	No				
	2	371	4.5	L	Black	No				
	4	371	8.5	L	Black	No				

*See last page of table for footnotes.

TABLE 2.2-4 (Continued)

STATIC THERMAL STABILITY COMPARISONS OF SELECTED ORGANIC FLUIDS

Compound (freezing point and normal boiling point, °C)	Length of Test (weeks)	Temp. (°C)	Sample Lost-%	Physical State[a*]	Color	Gas Chromatographic Analysis: Residual Pressure[b*]	Weeks at °C	% Lights[d*] (L)	% Higher[e*] (H)	Σ % L+H
4,4-diethyldiphenyl ether	0	-	-	L	Yellow	--				
(not available)	4	343	3.7	L	Yellow	No				
	2	371	12.0	L	Black	Yes				
Triethyldiphenyl ether	0	-	-	L	Yellow	--				
(isomer mixture)	2	371	13.6	L&S	Black	Yes				
(not available)	4	371	36.9	L&S	Black	Yes				
4,4-di-sec-butyl diphenyl ether	0	-	-	L	Yellow	-				
(N.A., 374)	2	343	4.3	L	Brown	Yes	3,843			>50[f]
	3	343	7.0	L	Brown	Yes				
	4	343	32	L&S	Yes					
Dicyclohexyl diphenyl ether	0	-	-	L	Yellow	--				
(N.A., 418)	2	343	7.8	L	Brown	Yes				
	4	343	13.0	L	Black	Yes				
Dodecyldiphenyl ether	0	-	-	L	Yellow	--				
(7.2 pour point, 427)	2	343	15.0	L&S	Brown	Yes				
	4	343	36	L&S	Black	Yes				
Ethylbiphenyl[4]	0	-	-	L	Colorless	--				
(-51 pour point, 280)	2	343	1.5	L	Yellow	No				
	4	343	3.9	L	Yellow	No				
	3	371	4.0	L	Brown	Yes				
	2	399	9.5	VL	Brown	Yes				
Partially Hydrogenated terphenyl[5]	0	-	-	L	Yellow	--				
(-26.1 pour point, 366)	8	343	2.5	L	Brown	No	8,343	3.4	1.5	4.9
	2	371	10.6	L	Brown	No	1,413	41.0	2.8	43.89
	4	371	10.3	L	Brown	Yes				

TABLE 2.2-4 (Continued)

STATIC THERMAL STABILITY COMPARISONS OF SELECTED ORGANIC FLUIDS

Compound (freezing point and normal boiling point, °C)	Length of Test (weeks)	Temp. (°C)	Sample Lost-%	Physical State[a*]	Color	Residual Pressure[b*]	Gas Chromatographic Analysis: Weeks at °C	% Lights[d*] (L)	% Higher[e*] (H)	Σ % L+H
	2	385	9.4	L	Brown	Yes				
	4	385	11.9	L	Black	Yes				
	1	399	42.7	L&S	Black	Yes				
Aliphatic oil[6]	0	-	-	L	Yellow	--				
(-9.4, 382-510)	2	343	8.3	L	Brown	No	2,343	9	7	16
	4	343	57.6	L&S	Brown	Yes	4,343	85	-	>85
Alkylaromatic oil[7]	0	-	-	L	Brown	--				
(-6.7, 343)	2	343	8.5	L	Brown	Yes	2,343	14	12	26[i]
	4	343	77.2	L&S	Brown	Yes	4,343	6	21	>27[i]

a - Physical state L = Liquid, S = Solid, V = Viscous
b - Residual pressure in reactor at dry ice temperature (-70°C)
c - Range of losses for several samples
d - Components boiling lower than fresh samples
e - Components boiling higher than fresh samples
f - High level of torr precluded accurate g.c. analysis. Value is minimal total degradation.
g - 57% of sample lost due to volatile products. Analysis is of remaining sample
h - 58% of sample lost due to volatile products. Analysis is of remaining sample
i - Sample lost at 2 weeks, 10%. Sample lost at 4 weeks, 77%. Analysis is of remaining sample.

[1]Dowthern A
[2]Dowtherm G
[3]Diphyl DT, Bayer, Germany
[4]Therm-S-600, Yawata Chemical Company, Japan
[5]Therminol 66
[6]Humbletherm 500
[7]Mobiltherm 600

TABLE 2.2-5. FLUIDS SURVIVING 382°C (720°F) STABILITY TEST FOR 24 HOURS OR LONGER

Fluid	Structure	Hrs Survival	Critical Temperature, °C[a]
Pyrazine		192	(352)[b]
Toluene	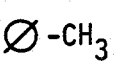	>336	320.8
Benzene		>336	288.9
Pyridine		336	346.8
Hexamethyldisilane	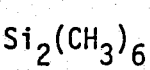	120	(334)
Thiopene		72	307
2-methylpyridine	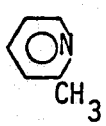	264	348
3-methylpyridine	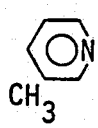	240	371.7
4-methylpyridine	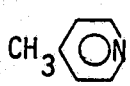	216	372.5
2,6-dimethylpyridine	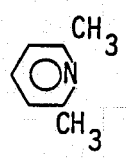	216	350.6
2-methyl pyrazine	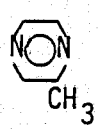	72	(368)[b]

[a] HCP

[b] Calculated

TABLE 2.2-6. SURVIVAL TIME OF FLUID MIXTURES AT 382°C (720°F)

Mixture	Mole Fraction Tested	Hrs Survival
ethanol-water	0.5:0.5	<24
n-propanol-water	0.5:0.5	<24
pyridine-water	0.5:0.5	>240
3-methylpyridine-water	0.5:0.5	216
pyrazine-water	0.25:0.75	<24
2-methylpyridine-water	0.5:0.5	>240
4-methylpyridine-water	0.5:0.5	>240
2,6-dimethylpyridine-water	0.5:0.5	>240
2-methylpyrazine-water	0.5:0.5	48

of destruction of the alcohol-water mixtures, as the samples were heated. Aromatic rings like the pyridine, benzene, and napthalene are fairly inert to such oxidation.

The general conclusions that can be made about thermal stability of non-halogen organic compounds are:

1. Totally aromatic compounds are the most stable (benzene, napthalene, biphenyl, etc.)

2. Aromatic ethers and simple alkylated aromatics (toluene) have good stability. Large alkyl groups or aromatics are not highly stable.

3. Molecular symmetry is usually beneficial to stability. Diphenyl ether is more stable than biphenylylphenyl ether.

4. Saturated alkyl compounds have poor thermal stability.

2.3 Halogenated Hydrocarbons

2.3.1 Halogenated Alkanes

Existing halogenated straight-chain hydrocarbons in general are not expected to be satisfactory heat pipe working fluids above 100-150°C. Not only are the bond dissociation energies for these halogenated species equal to or less than the corresponding hydrogen bond strengths (Table 2.2-1), but in addition, existing data show that they are particularly susceptible to catalytic decomposition. In a series of static capsule tests, F. J. Norton [19] found the decomposition of refrigerants R-12 and R-22 increased by a factor of 10^6 to 10^{10} in the presence of iron and copper oxides. This result is shown for R-22 in Figure 2.3-1, and for both R-12 and R-22 in Table 2.3-1 at various temperatures. In Table 2.3-1, the time required for 0.1% decomposition is shown for clean R-12 and R-22 as well as for these fluids in contact with oxides. Although R-12 and R-22 cannot be used as heat pipe fluids over the temperature range 100°C to 350°C, their chemical behavior is expected to be typical of halogenated straight-chain hydrocarbons with lower vapor pressures.

In the absence of oxides, a maximum operating temperature of about 200°C (392°F) is indicated for R-22, and a temperature in excess of 250°C (482°F) for R-12. In the presence of oxides, maximum operating temperatures become less than 100°C (212°F) and about 125°C (275°F) respectively for R-22 and R-12. In the cited tests by Norten, about 4 grams of oxide were used for a 0.2 gram gas charge, so that the tests were quite severe. However, the point remains that stabilities based on gas-phase pyrolysis establish an upper limit on working fluid operating temperature, but envelope reactions can reduce the maximum service temperature significantly.

The dominance of wall-induced decomposition on "high-temperature" refrigerants is also shown in the data of Callighan [20] in Figure 2.3-2. Callighan was investigating the stability of R-114 and R-216 for potential intermediate temperature turbine applications. In Figure 2.3-2, the results of three independent tests of R-114 and R-216 are presented as pounds of working fluid

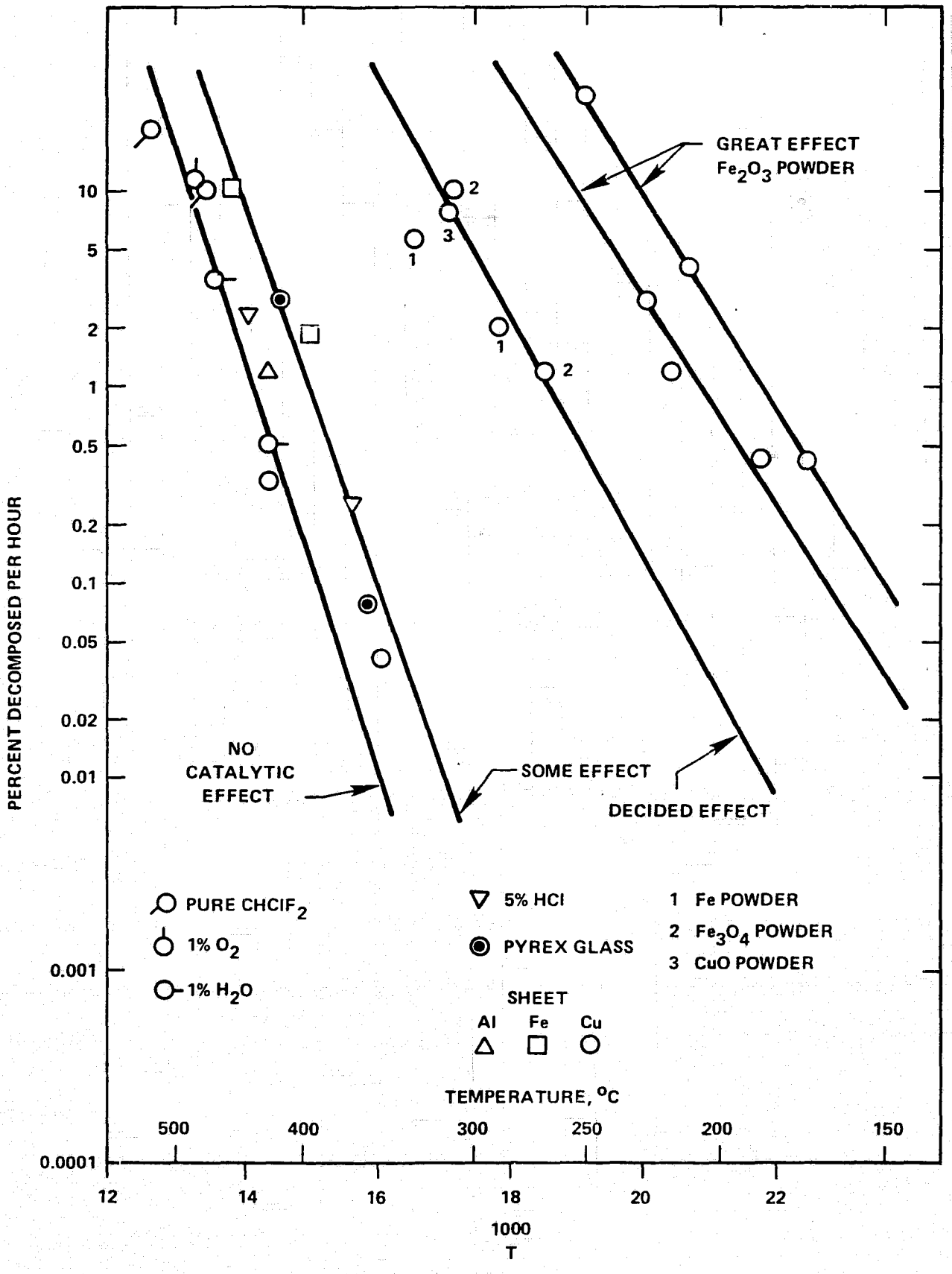

FIGURE 2.3-1. THE EFFECT OF VARIOUS ADDITIVES ON THE DECOMPOSITION OF R-22

TABLE 2.3-1. THE TIME REQUIRED FOR 0.1% DECOMPOSITION OF HALOCARBONS R-12 AND R-22 UNDER VARIOUS CONDITIONS[1]

Temperature (°C)	R-12 (yr)	R-12 + Fe_2O_3	R-22 (yr)	R-22 + OX.1[(2)]	R-22 + Fe_2O_3
100	$1.8(10^{16})$	730 yr	$4\ (10^{8})$	1.2 yr	5.8 days
150	$4.1(10^{11})$	11 mo	$1.6(10^{5})$	4.9 days	2.2 hrs
200	$9.1(10^{7})$	1.7 days	340	--	--
250	$9.9(10^{4})$	--	2.3	--	--

(1) From Norten, Ref. 19.

(2) Materials of similar activity: Fe Powder, Fe_3O_4 powder, and CuO powder.

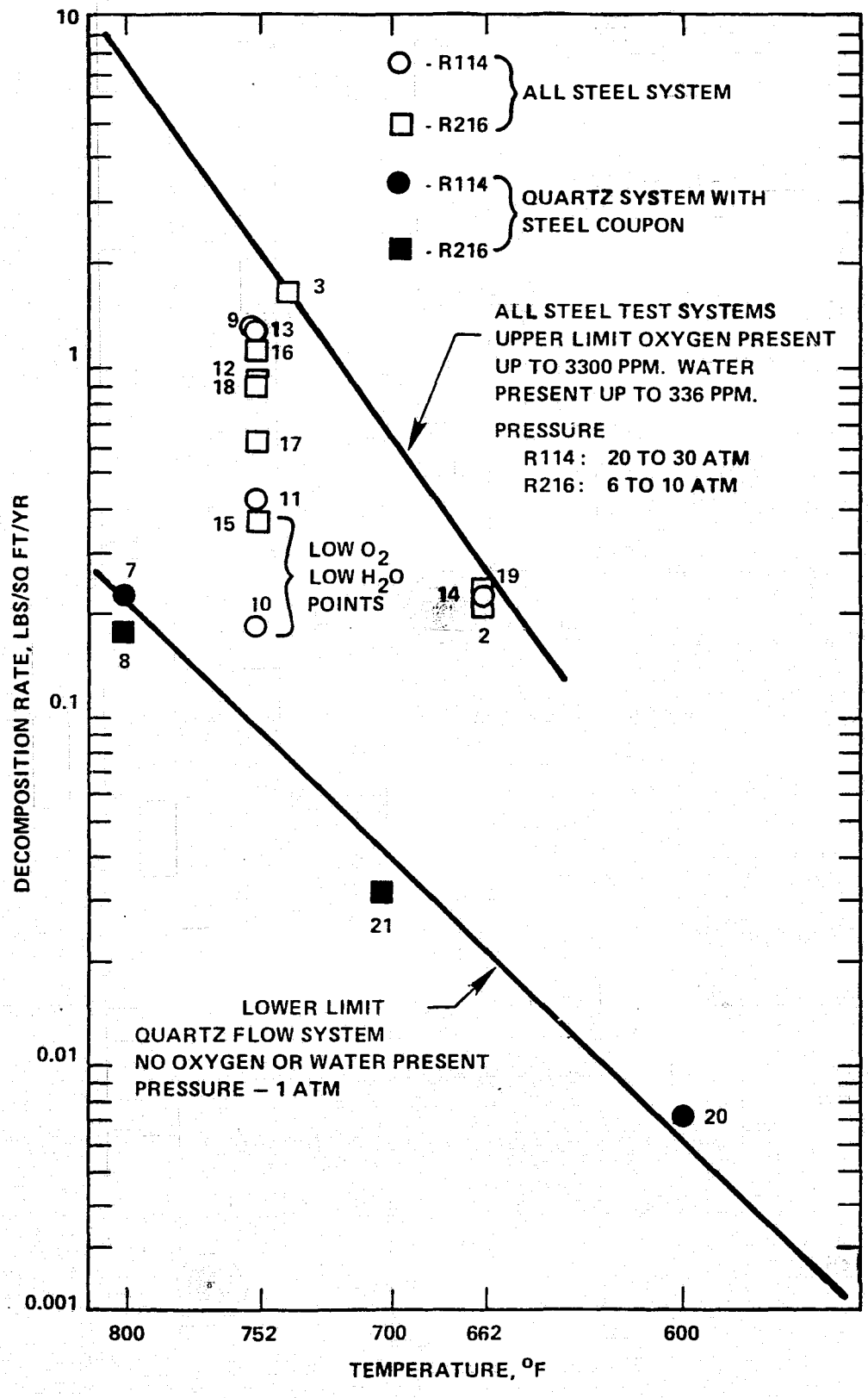

2.3-2. DECOMPOSITION RATE OF R114 AND R216 USING THREE DIFFERENT APPARATUS

decomposed per year per square foot of area. As shown, the use of a steel enclosure or steel coupons increased the decomposition rate at a given temperature by a factor of 10 to 20 beyond an all-quartz system. At an operating temperature of 315°C (600°F), for example, a steel system decomposition rate of 0.04 lb/sq ft/yr is indicated. This is quite high and unacceptable for heat pipes operating in this temperature range. If each mole of decomposing working fluid were to produce a mole of noncondensable gas, this is equivalent to about 2 liters of gas (STP) per square foot per year.

However, these specific fluids could not be operated at 300°C since the critical temperatures are 145.7°C and 180°C for R-114 and R-216. The primary point to be made is that the halogenated straight-chain hydrocarbons are susceptible to wall-dominated decomposition and have a maximum service temperature in the range of 100 to 200°C. Table 2.3-2 is a summary of the physical characteristics of R-114 and R-216.

Table 2.3-3 presents data from Dupont[21] on the maximum service temperatures for various halocarbon intermediate temperature working fluids. These data are basically in agreement with other data cited here. The effects of various metals on halocarbon decomposition have also been investigated for R-11 at 249°C, and these data are presented in Table 2.3-4. Other straight-chain halocarbons can be expected to behave qualitatively like R-11 with regard to catalytic decomposition. The catalytic effects of metals on halocarbon working fluids are as follows, progressing from high activity to low activity:

silver > steel > nickel > 18-8 stainless > Inconel > platinum

Aluminum is generally regarded as more active than steel and less active than silver. Copper is intermediate to nickel and steel. It is difficult to generalize this activity series to other working fluid families because the catalytic behavior is related in a complex way to temperature and pressure, to the relative strengths of chemical bonds, the type of molecular hybridization, and intermediate species. However, the ferrous metals and their oxides do display catalytic activity in a wide variety of chemical reactions.

TABLE 2.3-2. PHYSICAL PROPERTIES OF HALOCARBONS R-114 AND R-216

Characteristic	Value	
	R-114	R-216
Molecular weight	170.93	220.93
Heat of vaporization at boiling point, Joules/gm	246.5	211.4
Boiling temperature, ^{o}C	3.55	35.7
Freezing point, ^{o}C	-93.9	-125.4
Viscosity, centipoise	0.36 ($30^{o}C$)	0.5 ($20^{o}C$)
Density at $20^{o}C$, g/cm^3	1.47	1.57
Saturated vapor at 100 psig	$73.1^{o}C$	$114.4^{o}C$
Saturated vapor at 300 psig	$122.8^{o}C$	$165.5^{o}C$
Critical pressure, psia	474	399.45
Critical temperature, ^{o}C	145.7	180.0
Structural formulas	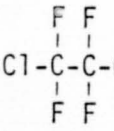	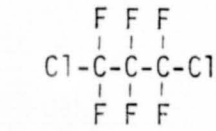

TABLE 2.3-3. DECOMPOSITION TEMPERATURES FOR HALOCARBON REFRIGERANTS IN THE PRESENCE OF STEEL

Fluid	Decomposition Rate Percent Per Year	
	0.1	1.0
R-11	89°C	129°C
R-12	100	145
R-113	91	137
R-114	97	146

TABLE 2.3-4. THE INFLUENCE OF METALS ON DECOMPOSITION OF R-11 AT 249°C

Metal	Decomposition Rate Percent Per Year
Silver	1500
Steel	120
Nickel	110
18-8 Stainless	20
Inconel	3
Platinum	1

2.3.2 Halogenated Aromatic Compounds

For the halogenated hydrocarbons, it is a general rule that the σ bond strengths are in the order F > Cl > Br > I. The most stable compounds are therefore expected to be the fluorocarbons, followed by the chlorocarbons. The σ bond resulting when chlorine is substituted for hydrogen in benzene is 25 Kcal/mole weaker than the original C-H bond, and the bond dissociation data of Table 2.2-1 indicate that the chloride bonds in both alkane and aromatic halocarbons are of comparable strength and, hence, that the stability of chlorinated hydrocarbons may, in general, be unsatisfactory for high temperature two-phase processes. Dowtherm E, is an example of a commercially available chlorinated aromatic compound (O-dichlorobenzene) with a boiling point of 177.8°C and a maximum recommended working temperature of 260°C. Available data on Dowtherm E indicate that aluminum catalyzes the decomposition of Dowtherm E to form hydrochloric acid, which in turn may accelerate chloride-activated corrosion.[22] As will be discussed at a later point, chlorinated napthalene in carbon steel has been unsatisfactory as a working fluid, and may represent a similar decomposition situation.

While it is not clear that the chlorinated aromatic compounds will be of adequate stability, attractive heat pipe working fluids may result from fluoro substitutions in aromatic compounds; from Table 2.2-1, an increase of about 13 Kcal/mole in bond strength is associated with substitution of fluorine for hydrogen in benzene.

Several of the halogenated aromatic compounds have thermophysical properties that would qualify them as potential working fluids for the 100°C to 350°C range. Hexafluorobenzene, for example, has a melting point of 5°C and a boiling point of 80.25°C, yet is considered to be thermally stable to a temperature of 650°C.[23] Various physical properties for C_6F_6 are summarized in Table 2.3-5. The liquid density at 25°C is 1.61 g/cm^3, and the surface tension is 21.8 dynes/cm. If a pressure of 15 atmospheres is considered the maximum safe working pressure, then this fluid is useable up to 195°C. Other possible halogenated aromatics include the fluoro- and chloronapthalenes. The Koppers Co. of Pittsburgh, Penn. makes a wide range of chlorinated napthalene materials that are used in such varied applications as sludge removal additives in petroleum

TABLE 2.3-5. PHYSICAL PROPERTIES OF HEXAFLUOROBENZENE[1]

Formula	-	C_6F_6
Molecular weight	-	186.06
Freezing point	-	$+5^{o}C$
Boiling point	-	$+80.25^{o}C$
Critical point	-	$243.2 \pm 0.4^{o}C$
Critical pressure	-	32.05 ± 0.71 atm.
Heat of vaporization at boiling point	-	32,700 J/g-mole
Surface tension	-	$24.62 - 0.113\ T$ (dynes/cm, ^{o}C)
Viscosity at boiling point	-	0.43 centipoise
Specific gravity	-	1.61 g/cm^3 at $25^{o}C$
Vapor pressure	-	$\log_{10}(P) = 4.37835 - 1386.88/(T + 238.03)$ (atm., ^{o}C)
Stability	-	thermally stable over $650^{o}C$
Toxicity	-	medium lethal air concentration for mice/2hrs = 95 mg/liter

(1) Derived from Reference 23.

oils and as high quality dielectric liquids and waxes.[24] The melting and boiling points of these materials are presented in Figure 2.3-3 as a function of chlorination level. It is quite remarkable that the addition of one chlorine molecule to napthalene drops the melting point of the material from 80.1°C (pure napthalene) to -25°C (monochloronapthalene), while the boiling point goes from 218°C to 250°C. Dichloronapthalene, on the other hand, has a melting point of about 60°C, and in this respect is similar to pure napthalene. These materials are relatively inexpensive, costing on the order of $1.00/lb. Unfortunately, Koppers Co. plans to halt production of these materials during 1977 because of excessive costs in meeting OSHA plant-site regulations[25] and Koppers Co. is presently the only U.S. company manufacturing the pure chlorinated napthalenes on a production basis.

Because of the unusual melting point depression with monochloronapthalene, it could be expected that monofluoronapthalene would show similar behavior.* This was found to be correct--the melting point of 1-fluoronapthalene is -9°C and its boiling point is 216°C. The fully halogenated compounds, however, differ in at least their melting points. The melting point of octafluoronapthalene ($C_{10}F_8$) is 87-88°C, which is much lower than a value of 185°C for octachloronapthalene.

Miller, et al.[26] have performed one of the most extensive series of tests on halogenated aromatic working fluids to date. In these tests, 0.5 to 2.0 cm^3 volumes of working fluid were sealed within 7 cm^3 low carbon steel capsules, and the capsules were then heated to 382°C. Periodically, the capsules were removed from test and examined for solids content, color, and acidity. The presence of "strong" acidity was considered to remove the fluid from consideration, while removal of fluids for solids content and color change was made on a qualitative visual examination. At 382°C, most of the fluids tested were apparently totally vapor, so that the tests represent the combined effects of gas phase pyrolysis and surface activated catalytic decomposition. The results of these tests are presented in Table 2.3-6 as hours of survival at 382°C. The survival times are in qualitative agreement with the relative bond strengths of chlorine and fluorine to benzene. The chloro compounds

* Mixtures of isomers

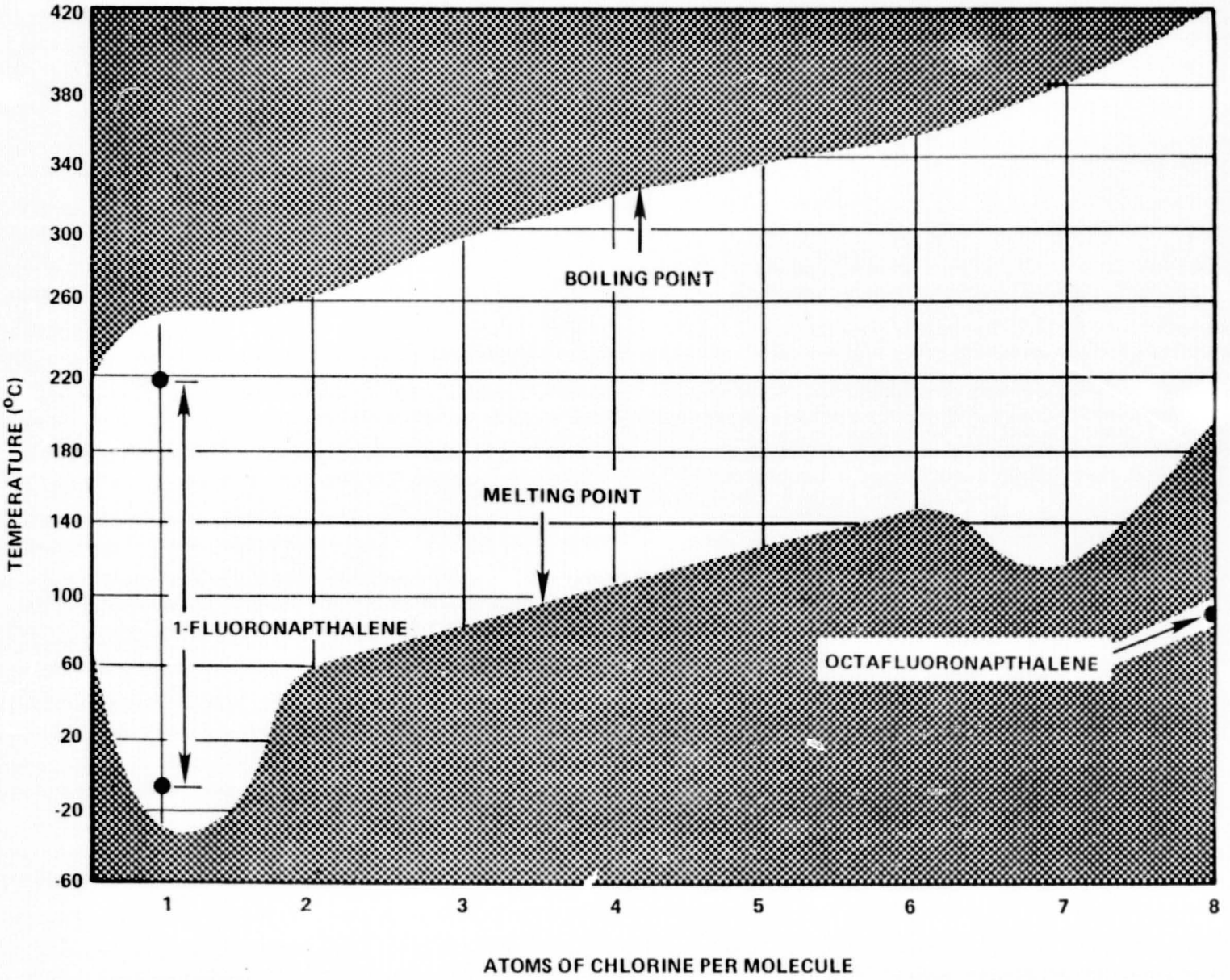

FIGURE 2.3-3. THE MELTING AND BOILING POINTS FOR CHLORINATED NAPTHALENE COMPOUNDS AS A FUNCTION OF DEGREE OF CHLORINATION. SIMILAR DATA FOR 1-FLUORONAPTHALENE AND

TABLE 2.3-6. FLUID SURVIVAL SUMMARY FOR 382°C STATIC CAPSULE TESTS[1]

Fluid	Hours Survival
benzotrifluoride	24
bromopentafluorobenzene	48
o-chlorofluorobenzene	48
m-chlorofluorobenzene	48
p-chlorofluorobenzene	24
chloropentafluorobenzene	48
1,2-dichlorohexafluorocyclobutane	120
o-difluorobenzene	>336
p-difluorobenzene	>336
m-difluorobenzene	>336
2,4-difluorotoluene	>240
2,5-difluorotoluene	>240
2,6-dimethylfluorobenzene	>240
2,3-dimethylfluorobenzene	>240
1,3-di(trifluoromethyl)benzene	>336
1,4-di(trifluoromethyl)benzene	24
fluorobenzene	>336
m-fluorobenzotrifluoride	72
o-fluorobenzotrifluoride	24
p-fluorophenyl trifluoromethyl ether	>192
o-fluorotoluene	168
p-fluorotoluene	168
m-fluorotoluene	168
hexafluorobenzene	>336
methylpentafluorobenzene	96
octafluorotoluene	>336
pentafluorobenzene	>336
perfluoro(methylcyclohexane)	>336

(1) From Reference 26. SAE 1008 low carbon steel tubes, 0.5 to 2.0 cm^3 fluid charges in a 7 cm^3 total volume.

TABLE 2.3-6. (Continued)

Fluid	Hours Survival
perfluoroalkane-70	96[2]
perfluorotributylamine	48[2]
perfluoro-2 butyltetrahydrofuran	144[2]
perfluoro(dimethylcyclohexane)	>336
phenyltrifluoromethyl ether	48
1,2,4,5-tetrafluorobenzene	>336
1,2,3,5-tetrafluorobenzene	>336
2,3,5,6-tetrafluorotoluene	24
1,2,4-trifluorobenzene	>336
1,3,5-trifluorobenzene	>336
2,2,2-trifluoroethanol	24
tris(trifluoromethyl)-s-triazine	24
monochlorobenzene	48
Allied P-ID perfluoroether	>336
N-nonafluorobutyloctafluoromorpholine	96
pentafluoropyridine	>336

survived on the order of 100 hours or less at 382°C, while most of the fluoro compounds survived in excess of 336 hours.

In applying this information to heat pipe fluid selection, it must be recognized that the survival times were based on fluid property changes that characteristically occur at much later times than are typical of corresponding heat pipe degradation phenomena. Specifically, the buildup of noncondensable gases via fluid decomposition is often a serious problem long before any significant change in fluid properties can be observed, and any sludge or tars produced will immediately become concentrated in the evaporator, leading to wick or groove clogging and uncertain fluid distribution. Therefore, Table 2.3-6 may present an optimistic view of heat pipe fluid stability.

Two other features of the experiments may influence the results in an unknown fashion. First, the fluids appear to be completely vapor at 382°C, and hence the normal two-phase condition within a heat pipe is not duplicated. Secondly, mention is made of the capsules being charged in air and subsequent tests being performed in air, so that there may be an effect of either fluid oxidation or oxygen-influenced surface decomposition.

2.4 Inorganic Fluids

In addition to the well-known inorganic fluids ammonia, sulfur dioxide, and water, there are a large number of other inorganic fluids that may be of interest in heat pipe applications. Inorganic working fluids for heat pipes can be characterized as either molecular or ionic liquids. In the molecular liquids, the inorganic molecule does not lose its structure in the solid/liquid transition, in analogy with most organic compounds. The ionic liquids, on the other hand, form a melt containing discrete positive and negative ions and molecular structure is destroyed. Many of the inorganic compounds of interest for heat pipe applications fall into the domain of molecular fluids at normal operating temperatures, although the distinction between molecular and ionic behavior becomes indistinct at higher temperatures where the probability for dissociation increases. In aqueous solutions, many halide salts accelerate the

corrosion of metal envelopes, but it is not necessarily true that the pure anhydrous halide molecular fluids will enhance the same corrosion mechanisms. The inorganic molecular fluids have solvent properties that are significantly different than water. In Section 2.4.1, the physical properties of inorganic fluids will be discussed, while in Section 2.4.2, the compatibility of halide working fluids with metal envelopes will be predicted on the basis of equilibrium chemical thermodynamics.

2.4.1 Physical Properties

Several inorganic molecular fluids have vapor pressure characteristics similar to water or intermediate to water and the liquid metals. Vapor pressure characteristics of selected inorganic fluids are presented in Figure 2.4-1. As will be shown below, most of the inorganic fluids are metal halides, and thermophysical data on these compounds are quite limited. In general, the fluids have thermal conductivities and surface tensions very similar to organic fluids. Liquid densities on the other hand are quite high, and the fluids will in general display rather poor priming capability in 1 g. This high density is of benefit in reflux devices since Nusselt films will be thinner and film temperature differences reduced.

A compilation of potential inorganic working fluids is given in Table 2.4-1. The table presents a brief outline of fluid properties including density at 20°C, and latent heat of vaporization at the boiling point. A limited amount of toxicity data is also presented. The toxicity scale ranges from 1 to 5. A material with a toxicity rating of 1 is essentially nontoxic while a material with a rating of 5 is highly toxic. The toxicity scale, derived from Reference 27, is specifically defined as follows:

1. No residual injury is to be expected from accidental exposure even if no treatment is applied.
2. Minor residual injury may result from some accidental exposures if no treatment is applied.
3. Minor residual injury may result in spite of prompt treatment.

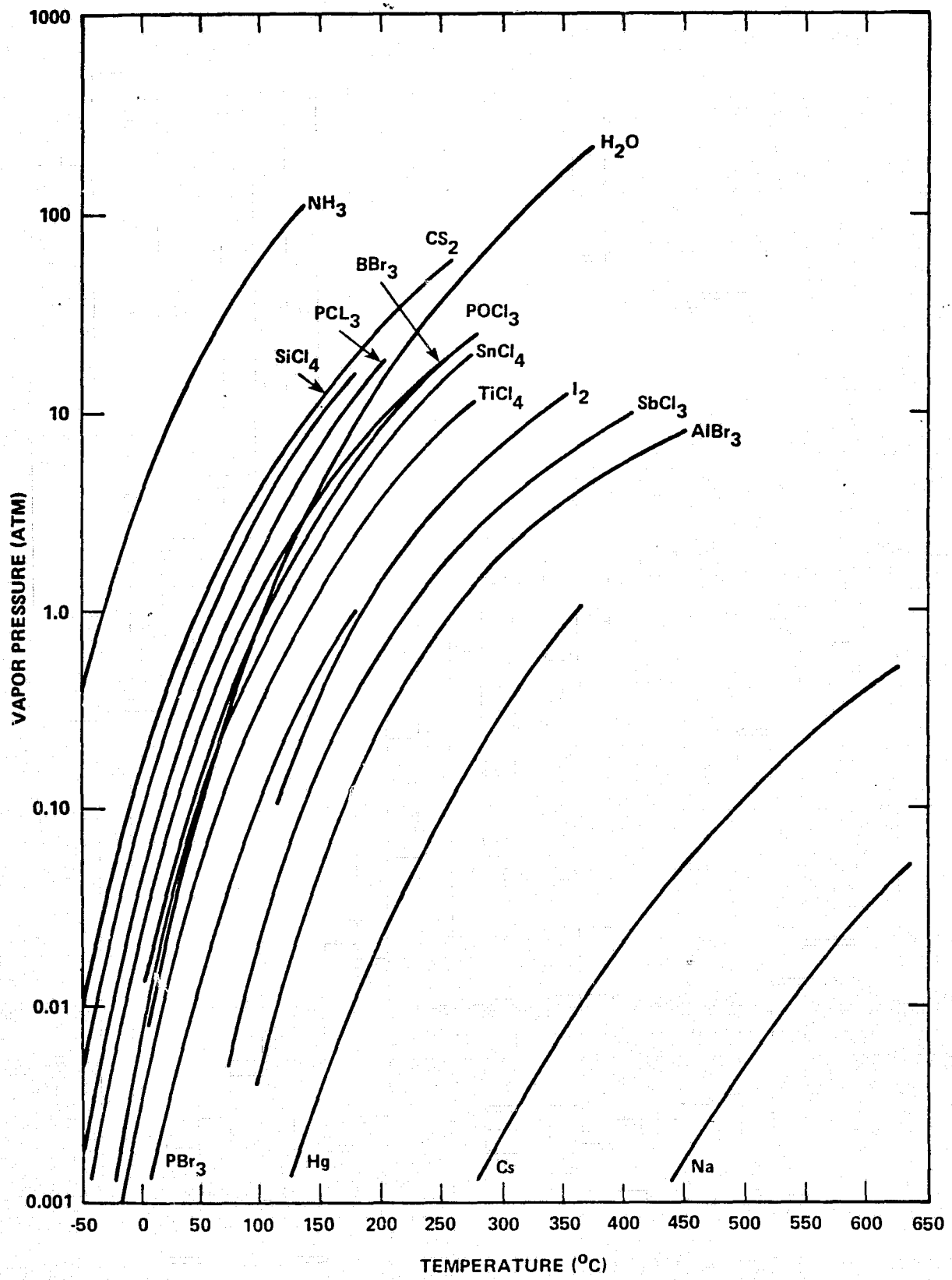

FIGURE 2.4-1. VAPOR PRESSURE OF VARIOUS INORGANIC LIQUIDS OF POTENTIAL INTEREST FOR HEAT PIPE APPLICATIONS

7706-232.8

TABLE 2.4-1. THERMOPHYSICAL AND TOXICITY BEHAVIOR OF POSSIBLE INORGANIC FLUIDS FOR TWO-PHASE HEAT TRANSFER APPLICATIONS

Name	Formula	Molecular Weight	Density	Melting Point(°C)	Boiling Point(°C)	$-\Delta G^{o}$ at 25° (Kcal/mole)	ΔH_{fg} (Joules/mole)	Toxicity						
								eye	inhal	skin pen	skin irrit	ingest	max ppm (air)	mg/m^3 (air)
Aluminum Bromide	$AlBr_3$	266.71	2.64	97.5	263.3	120.7c	46,931	Moderate, reacts with water						
Aluminum Chloride	$AlCl_3$	133.34	(1) 1.31	190	182.7	152.2c	39,652	5	--	--	3y	2		
Aluminum Iodide	AlI_3	407.69	3.98	191	360	75.0c	70,830	Moderate, reacts with water						
Ammonia	NH_3	17.03	0.7710 g/ml 760 mm	-77.7	-33.35	3.98g	24,670	4z	5z	--	3z	--	25	18
Ammonium bicarbonate	NH_4HCO_3	79.06	1.58	107.5	subl			Low hazard						
Ammonium Nitrate	NH_4NO_3	80.04	1.725	169.6	210	---		2x	1x	1x	1x	2x		
orthophosphate, di-H	$NH_4H_2PO_4$	115.03	1.803	190	---			(possible explosion hazard)						
Antimony Tribromide	$SbBr_3$	361.48	6.684	96.6	280	---	62,431	Antimony compounds dangerous if ingested or inhaled.						
Antimony Trichloride	$SbCl_3$	228.11	3.140	73.4	219	72.3g	49,188	Irritant. Releases HCl with water.						0.5
Antimony Pentafluoride	SbF_5	216.74	(1) 2.99	7	149.5									
Antimony Trifluoride	SbF_3	178.75	4.379	292	subl 319	---								
Antimony Tri-Iodide	SbI_3	502.46	4.917	170	401	---	68,550	Dangerous if ingested or inhaled.						0.5
Bismuth Tribromide	$BiBr_3$	448.71	(1) 4.4	218	453		75,976	Bismuth compounds less toxic than most. Hazards primarily associated with HCl						
Bismuth Tetrachloride	$BiCl_4$	350.79	---	225	---	---								
Bismuth Trichloride	$BiCl_3$	315.34	(1) 3.7	230-232	447	76.23c	71,786							
Boric Acid, meta-	HBO_2	43.82	2.486	236 ±1	---	170.5c		3x	2x	2x	1x	2		
Boron Tribromide	BBr_3	250.54	2.6431	-46	94.3±0.25	51.0g	35,430	Forms HBr with water. Can explode on decomposition.					1	10
Boron Trichloride	BCl_3	117.17	1.349	-107.3	12.5	94.5g	27,561	Corrosive, respiratory irritant.						

TABLE 2.4-1 (Continued)

Name	Formula	Molecular Weight	Density	Melting Point(°C)	Boiling Point(°C)	$-\Delta G^{o}$ at 25° (Kcal/mole)	ΔH_{fg} (Joules/mole)	Toxicity						
								eye	inhal	skin pen	skin irrit	ingest	max ppm (air)	mg/m^3 (air)
Boron Hydride	$B_{10}H_{14}$	122.22	0.94	99.5	213			Possible explosion hazard.						
Boron Tri-iodide	BI_3	391.52	3.35	49.9	210									
Bromine	Br_2	159.81	2.928	-7.2	58.78	-0.75g	32,294	5x	2x	1x	5x	--	0.1	0.7
Bromine Pentafluoride	BrF_5	174.90	2.466	-61.3	40.5	---	31,810	Corrosive, irritant to skin, mucous membrane.					0.1	0.7
Carbon Tetrabromide	CBr_4	331.65	3.42	48-90	189.5		41,462	Highly toxic.						
Carbon Tetrachloride	CCl_4	153.81	1.5867	-23	76.8		32,691	3x	5z	2	2x	2	10	65
Carbon Disulfide	CS_2	75.14	1.261	-110.8	46.3	-15.55	29,600	3x	5z	3x	2x	3x	20	60
Cesium	Cs	132.905	1.8785	28.5	690	0	72,450	5x	--	--	5x	--	fire hazard	
Cesium Pentaiodide	CsI_5	767.43	---											
Cesium Tri-iodide	CsI_3	513.62	4.47	207.5	---									
Gallium Dichloride	$GaCl_2$	140.63	---	164	535									
Gallium Trichloride	$GaCl_3$	176.03	2.47	77.9±0.2	201.3	170.5	47,620	Toxicity low for gallium bromide and iodide.						
Gallium Tribromide	$GaBr_3$	309.45	3.69	121.5±0.6	278.8									
Gallium Tri-iodide	GaI_3	450.43	4.15	212±1	subl 345									
Germanium Tetrabromide	$GeBr_4$	392.23	3.132	26.1	186.5	---	43,283	Germanium bromide toxicity low.						
Germanium Tetrachloride	$GeCl_4$	214.41	1.8443	-49.5	84	---	34,971	Only slight toxicity. Moderate irritant of eyes and skin.						
Indium Dibromide	$InBr_2$	274.64	4.22	235	632 subl								--	0.1
Indium Monobromide	InBr	194.73	4.96	220	662 subl			Indium compounds may be highly toxic.					--	0.1

TABLE 2.4-1 (Continued)

Name	Formula	Molecular Weight	Density	Melting Point(°C)	Boiling Point(°C)	$-\Delta G^{o}$ at 25° (Kcal/mole)	ΔH_{fg} (Joules/mole)	Toxicity: eye	inhal	skin pen	skin irrit	ingest	max ppm (air)	mg/m^3 (air)
Indium Tribromide	$InBr_3$	354.55	4.74	436±2	subl								--	0.1
Indium Dichloride	$InCl_2$	185.73	1.655	235	550-570								--	0.1
Indium Monochloride	InCl	150.27	4.19 (y) 4.18 (r)	225±1	608	23g							--	0.1
Indium Tri-iodide	InI_3	495.53	4.69	210	---								--	0.1
Iodine	I_2	253.809	4.93	113.5	184.35	-4.63g	45,420	5x	4x	3x	4x	4x	0.1	1.0
Iodine Pentafluoride	IF_5	221.90	3.75	9.6	98			Highly toxic and corrosive.						
Lithium Iodide	LiI	133.84	3.494 ±0.015	450	1180±10	26g	174,742							
Lithium Nitrate	$LiNO_3$	68.94	(1) 1.7	264	d 600			Relatively non-toxic.						
Magnesium Chloride	$MgCl_2$	95.22	2.316-2.33	708	1412	141.57c	140,602	2x	--	1x	2x	2		
Manganese Dichloride	$MnCl_2$	125.84	2.977	650	1190	105.5	131,510							
Mercury	Hg	200.59	13.5939	-38.87	356.58	-7.6g	60,261	Toxic vapor.					0.006	0.05
Molybdenum Pentachloride	$MoCl_5$	273.21	2.928	194	268			May form HCl with water.					--	5.0
Molybdenum Oxytetrafluoride	$MoIF_4$	187.93	3.001	98	180								--	5.0
Niobium Pentafluoride	NbF_5	187.90	3.293	72-73	236									
Nitrogen Peroxide	NO_2 (N_2O_4)	46.01	1.4494	-11.20	21.2	-12.39g (-2.31)	(33,950)	3x	5z	--	3x	--	5	9.0
Phosphorus Tribromide	PBr_3	270.70	2.852	-40	172.9	41.2g	41,500	Toxic and corrosive.						
Phosphorus Dichloride	PCl_2	101.88	---	-28	180									

TABLE 2.4-1 (Continued)

Name	Formula	Molecular Weight	Density	Melting Point(°C)	Boiling Point(°C)	$-\Delta G^{o}$ at 25° (Kcal/mole)	ΔH_{fg} (Joules/mole)	Toxicity						
								eye	inhal	skin pen	skin irrit	ingest	max ppm (air)	mg/m^3 (air)
Phosphorus Trichloride	PCl_3	137.33	1.574	-112	75.5	68.42g	33,540	Irritant					0.5	3.0
chloride(di)-nitride	$(PNCl_2)_3$	347.66	1.98	114	256.5									
chloride(di)-nitride	$(PNCl_2)_4$	463.55	2.18	123.5	328.5									
Phosphorus Sesquioxide	P_4O_6	219.89	2.135	23.8	175.4									
Phosphorus Trioxide	P_2O_3	109.95	2.135	23.8	173.8 (in N_2)		43,080	Caustic						
Phosphorus Oxybromide	$POBr_3$	286.70	2.822	56	189.5			Oxyhalogens produce acids on decomposition with water.						
oxydibromide chloride	$POBr_2Cl$	242.27	(1) 2.45	30	165									
oxybromide chloride, di	$POBr_2Cl_2$	197.79	(1) 2.104	13	137.6									
Phosphorus Oxychloride	$POCl_3$	153.33	1.675	2	105.3									
(tetra)sulfide,hepta	P_4S_7	348.34	2.19	310	523									
Phosphorus Pentasulfide	P_2S_5	222.27	2.03	286.90	514			Irritant. Forms H_2S with water.						
Selenium	Se	78.96	4.81	217	684.9±1.0	18.77	93,850	Low systemic toxicity.						
Selenium Chloride	$SeCl_2$	102.98	2.682	45.5	125-126								--	0.2
Silicon Tetrabromide	$SiBr_4$	347.72	(1) 2.7715	5.4	154	---		Produces HBr on thermal decomposition in air.						
(di)bromide, hexa..	Si_2Br_6	535.62	---	95	240									
Silicon Tetrachloride	$SiCl_4$	169.90	(1) 1.483	-70	57.57	136.2g	32,000	Produces HCl when heated to decomposition in air. May be irritant to mucus membranes.						
(di)chloride,hexa..	Si_2Cl_6	268.89	1.58	-1	145	---	45,964							
Silicon Tetraiodide	SiI_4	535.70	4.198	120.5	287.5	---		Moderate skin irritant. Dangerous when heated to decomposition.						
Sodium Amide	$NaNH_2$	39.01	---	210	400			Moderate toxicity. Moisture liberates NH_3 and NaOH.						

TABLE 2.4-1 (Continued)

Name	Formula	Molecular Weight	Density	Melting Point(°C)	Boiling Point(°C)	$-\Delta G^{o}$ at 25° (Kcal/mole)	ΔH_{fg} (Joules/mole)	Toxicity						
								eye	inhal	skin pen	skin irrit	ingest	max ppm (air)	mg/m^3 (air)
Sulfur (α)	S_8	256.512	2.07	112.8	444.6	-43.57g	71,262	Low toxicity.						
Sulfur (β)	S_8	256.512	1.96	119.0	444.6									
Sulfur (γ)	S_8	256.512	1.92	ca 120	444.6									
Sulfur Trioxide (α)	SO_3	80.06	1.97	62.3	44.8	88.52	42,520	Irritant. Dangerous if inhaled or ingested.						
Sulfur Trioxide (β)	SO_3	80.06	---	32.5	44.8	---	42,520							
Sulfur Trioxide (γ)	SO_3	80.06	(1) 1.920	16.8	44.8									
Tin (II) Bromide	$SnBr_2$	278.51	5.117	215.5	620								--	2.0
Tin (IV) Bromide	$SnBr_4$	438.33	(1) 3.34	31	202	---	45,912	Moderate toxicity unless heated to decomposition.					--	2.0
Tin (IV) Chloride	$SnCl_4$	260.50	(1) 2.226	-33	114.1	113.31	39,770	HCl liberated with water or high temp.					--	2.0
Tin Iodide	SnI_2	372.50	5.285	320	717									
Tin (IV) Iodide	SnI_4	626.31	4.473	114.5	364.5									
Titanium Tetrabromide	$TiBr_4$	367.54	2.6	39	230									
Titanium Dichloride	$TiCl_2$	118.81	3.13	subl H_2	d 475 vac									
Titanium Di-iodide	TiI_2	301.71	4.99	600	1000									
Tetra-iodide	TiI_4	555.52	4.3	150	377.1									
Water	H_2O	18.01534	1.00	0.00	100.0	54.64g	43,000	Non-toxic.						
Zinc Bromide	$ZnBr_2$	225.19	4.201	394	650	74.142c								
Zinc Chloride	$ZnCl_2$	136.28	2.91	283	732	88.26	120,000	5x	--	2x	4x	3x (used as a supplement food add.)	--	1.0

4. Major residual injury may result in spite of prompt treatment.

5. Major residual injury is likely in spite of prompt treatment.

x. Entry based upon analogy with a closely similar structure, or on other estimate believed sound.

y. Entry based on a nonstandard test (a test different from the usual test described for each type of contact).

z. Entry based upon human experience, superseding animal data.

The maximum parts per million in air is the so-called threshold limit value, representing "... conditions under which it is believed that nearly all workers may be repeatedly exposed day after day without adverse effect."(28)

The inorganic molecular fluids as a class are quite stable. The free energies of formation at 25°C for many of the compounds exceed -100 Kcal/g-mole, while in comparison, most of the straight-chain hydrocarbons have free energies in the range of -5 to -30 Kcal/g-mole. Carbon disulfide is a notable exception with a +15.55(g) free energy of formation, i.e., CS_2 is thermodynamically unstable. However, the rate of carbon disulfide decomposition cannot be calculated from free energy data and it is possible to store CS_2 at room temperature for long periods of time without noticeable decomposition. With many of the inorganics, including CS_2, a further benefit is realized: noncondensable gases will not form upon decomposition of the working fluid.

The majority of inorganic fluids of possible interest are metal halides. It is difficult to generalize the halide physical properties. Melting and boiling points are extremely variable and toxicities range from high to moderate. The latent heat of vaporization ranges from 30,000 Kcal/g-mole to over 100,000 Kcal/g-mole at the boiling point. Liquid densities are high, ranging from about 1.5 g/cm^3 to more than 5 g/cm^3. Many of the fluids are hygroscopic and react with water vapor to form the corresponding halogen acid and metal oxide. In the following section, the metal halide working fluids are discussed in more detail, and in particular, chemical reactions of the working fluid with the envelope are considered.

2.4.2 Inorganic Fluid/Envelope Stability

On the basis of free energies of formation, many inorganic fluids are expected to be inherently more resistant to thermal degradation than organic fluids. However, this is for the situation in which working fluid vapor is contained within an inert container. When actual operating conditions are considered, it is apparent that chemical reactions between the working fluid and the container (heat pipe envelope) may place considerable restrictions on fluid selection. The molecular fluid water, for example, is extremely stable, yet is known to generate hydrogen in envelopes made with metals high in the electromotive series. The electromotive series is useful for predicting the probability of a chemical reaction in water, but it is not applicable to non-aqueous systems because the presence of water as a solvent influences the chemical equilibrium. To define a similar factor that predicts the probability of reaction between an inorganic fluid and a metal envelope, the relative stability of the fluid and metal envelope halides must be compared. Because so many of the potential working fluids are metal halides, the following analysis is specifically for metal chlorides; generalization to other compounds is straightforward.

For an inorganic molten halide salt M_bX_{cn} in contact with a wall composed of metal M_a, the following double displacement reaction may occur depending on the relative chemical activities of the two halide salts:

$$fM_a + gM_bX_c \rightleftarrows fM_aX_{cp} + gM_b \qquad (2.4\text{-}1)$$

A typical example is the reaction of iron with bismuth trichloride,

$$Fe(s) + BiCl_3(\ell) \rightleftarrows FeCl_3(s) + Bi(s) \qquad (2.4\text{-}2)$$

In this case, iron in the heat pipe envelope is postulated to have a greater affinity for chloride than does the bismuth contained in the working fluid, with the subsequent production of iron chloride (III) and metallic bismuth.

A reaction written as equation (2.4-1) will have a free-energy change given by

$$\Delta G = \Delta G^{o} + RT \ln \left[\frac{\left(a_{M_a} X_{cp}\right)^{f} \left(a_{M_b}\right)^{g}}{\left(a_{M_a}\right)^{f} \left(a_{M_b} X_{c}\right)^{g}} \right] \qquad (2.4\text{-}3)$$

where a_p^Q is the chemical activity of the "p" constituent in the balanced chemical equation with multiplier "Q". The free-energy change when all chemical activities are equal to unity is ΔG^{o}. Similarly, the corresponding electromotive force difference ΔE for this reaction is

$$\Delta E = \Delta E^{o} - \frac{RT}{nF} \ln \left[\frac{\left(a_{M_a} X_{cp}\right)^{f} \left(a_{M_b}\right)^{g}}{\left(a_{M_a}\right)^{f} \left(a_{M_b} X_{c}\right)^{g}} \right] \qquad (2.4\text{-}4)$$

where ΔE^{o} is the electromotive force difference when all reactants are at unit chemical activity, and where "n" is the number of electrons transferred in the balanced equation. The factor F is the Faraday, equal to Avogardro's number of electrons (23.06 Kcal/volt g-mole). Unit chemical activity is usually taken as the pure material at 1 atmosphere pressure. The standard electromotive force difference ΔE^{o} is given by

$$\Delta E^{o} = \frac{-\Delta G^{o}}{nF} \qquad (2.4\text{-}5)$$

The corrosion potential ΔE, or free-energy change ΔG, requires a physical model so that the various chemical activities can be appropriately defined. In Figure 2.4-2, a hypothetical corrosion cell is depicted for the $Fe/BiCl_3$ combination. If reaction (2.4-2) has a large negative energy of formation, then it can be expected that the reaction from left to right is spontaneous, and $FeCl_3$ and free bismuth will be favored. However, the solubility of a metal in a dissimilar metal halide melt is generally small,[29] and it can be assumed that the $FeCl_3$ will form a film over some fraction of the surface,

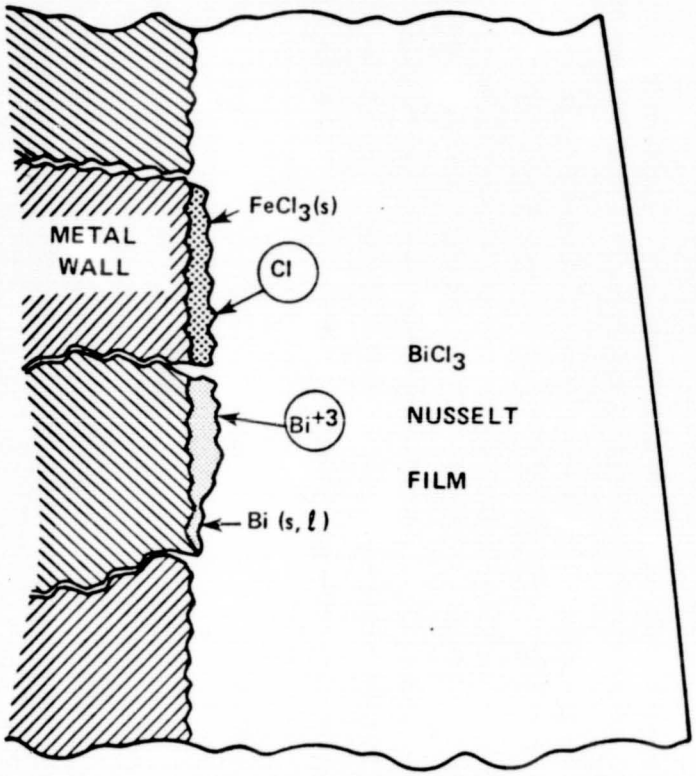

OVERALL REACTION: $BiCl_3(\ell) + Fe(s) \rightarrow Bi(s) + FeCl_3(s)$

FIGURE 2.4-2. HYPOTHETICAL REACTION CELLS FOR CORROSION OF IRON BY A FILM OF MOLTEN BISMUTH TRICHLORIDE

7706-232.6

and that the bismuth will also be deposited on the iron surface in preferential locations. Each corrosion cell so defined

$$Fe,\ FeCl_3;\ BiCl_3\ (\ell);\ BiCl_3,\ Bi$$

One electrode of the cell is the combination Fe, $FeCl_3$, while the other electrode is $BiCl_3$, Bi. The electrodes are coupled by ionic conduction in the liquid bismuth chloride. If the solubility of iron and bismuth trichloride in bismuth is neglected, and the solubility of $BiCl_3$ in $FeCl_3$ is neglected, then the activities of the various constituents are all approximately unity, and $\Delta E = \Delta E^o$ and $\Delta G = \Delta G^o$. It is useful to estimate the error in this series of approximations. For the bismuth trichloride/iron system, if for example, the ratio of activities in equations (2.4-3) or (2.4-4) equals 2.00 in value, the cell potential at 25°C changes by

$$\Delta E = \Delta E^o - \frac{1.987\ (298.15)}{3 \cdot 23{,}060}\ \ell n\ 2 = \Delta E^o - 0.0059 \quad \text{(volts)} \qquad (2.4\text{-}6)$$

Electromotive potential differences change on the order of 0.005 to 0.010 volts for each factor of two change in the logarithmic component of equation (2.4-4). This is a relatively small effect.

The physical state of the $FeCl_3$ and bismuth deposits has not been addressed. There is the possibility, depending on temperature, that one or another of the components will be a liquid rather than a solid. The phase change in itself will not influence ΔE^o, since a solid-to-liquid transition occurs with zero change in free energy [Reference 30 and equation (2.4-5)]. There can, of course, be significant changes in mutual solubilities and diffusivities on melting, and these physical system effects are not included in this model.

It is also true that one of the constituents may grow over the contacting interface at the expense of other constituents. For example, if the bismuth is molten, it will tend to spread over the iron by surface tension forces,

displacing iron chloride. This will tend to ultimately passivate the surface, although there may be local areas where significant pitting occurs as the anode/cathode area ratio changes.

Decomposition Potentials

It has been shown that the corrosion of a heat pipe envelope by an inorganic halide working fluid is dependent on the free-energy change ΔG^o when the working fluid (M_bX_c) and wall (M_a) participate in a double displacement reaction

$$fM_a + gM_bX_c \rightleftarrows fM_aX_{cp} + gM_b \qquad (2.4\text{-}7)$$

The free energy change corresponds to a potential difference ΔE^o given by equation (2.4-5).

The EMF of reaction (2.4-7) can be readily found using decomposition potentials characteristic of the decomposition of the working fluid compound M_bX_c and the metal wall halide M_aX_{cp}. These correspond to

$$M_a;\ M_aX_{cp};\ X_2 \qquad (2.4\text{-}8)$$

$$M_b;\ M_bX_b;\ X_2 \qquad (2.4\text{-}9)$$

where X_2 is the halide gas. Neglecting polarization effects, the decomposition potential E_p is the voltage that must be applied to inert electrodes in an inorganic halide to produce metal and halide gas at unit concentration. Fluids with a high decomposition potential are more inherently stable than fluids with a low decomposition potential.

The decomposition potentials for a large number of chlorides are presented in Figure 2.4-3 as a function of temperature.[31,32] These values are a mixture of empirical data and theoretical estimates. The values at 25°C were calculated by the present author from data in Reference 33, and were coupled to the values of Delimarskii and Markov[31] by a straight line extending from 25°C to their lowest temperature estimates of E_p. The standard EMF for a given

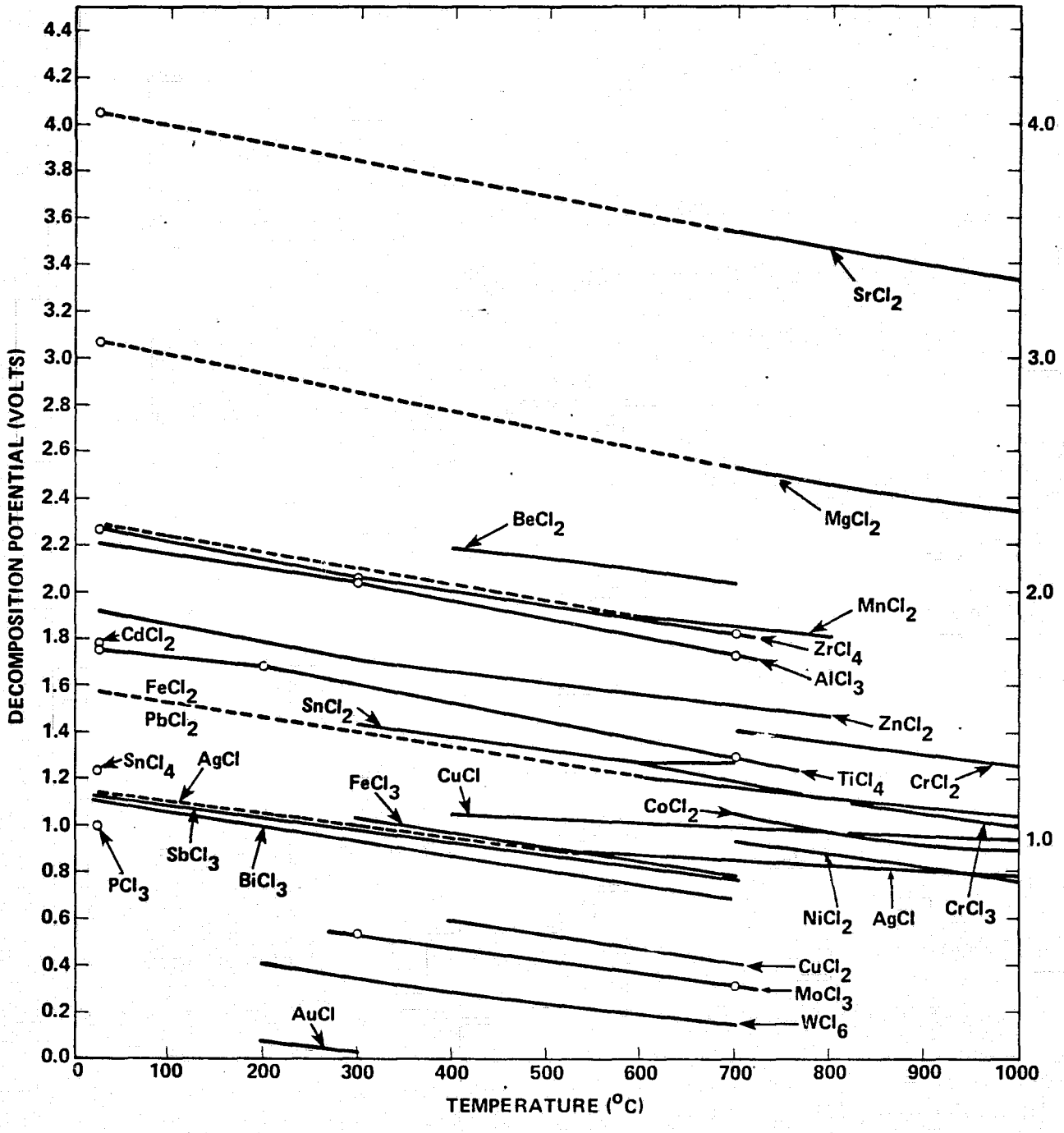

FIGURE 2.4-3. DECOMPOSITION POTENTIALS FOR VARIOUS INORGANIC CHLORIDES

7706-232.5

halide/metal reaction of the type given in equation (2.4-7) is

$$\Delta E^{o} = E_p \text{ (product halide)} - E_p \text{ (initial halide)} \qquad (2.4\text{-}10)$$

If the standard EMF, ΔE^{o}, is positive, then the reaction can proceed spontaneously and the wall will react chemically. If the standard EMF is strongly negative, then reaction of the wall material with the working fluid will not be as significant, although a limited reaction is not precluded.

Example 1

The chemical cell potential of $BiCl_3$ fluid in an iron heat pipe at 400°C is governed by the equation

$$Fe(s) + BiCl_3\,(\ell) \rightarrow FeCl_3(s) + Bi(s) \qquad (2.4\text{-}11)$$

At an operating temperature of 400°C, Figure 2.4-3 shows that

$$\text{cell potential} = E_p(FeCl_3) - E_p(BiCl_3)$$

$$= 0.965 - 0.870$$

$$= +0.095 \text{ volt}$$

Hence, the reaction should spontaneously proceed towards iron chloride (III) and bismuth metal.

Example 2

The corrosion of an iron heat pipe by liquid $TiCl_4$ at 250°C may be governed by the equation

$$2Fe(s) + TiCl_4(\ell) \rightarrow 2FeCl_2(s) + Ti(s) \qquad (2.4\text{-}12)$$

The cell potential for this postulated reaction is

$$\Delta E^{o} = E_p(FeCl_2) - E_p(TiCl_4)$$

$$= 1.43 - 1.64$$

$$= -0.21 \text{ volt}$$

The reaction represented by equation (2.4-12) is not spontaneous. The components of equation (2.4-12) are actually not at unit activity because the vapor pressure of $TiCl_4$ at $150^{o}C$ is on the order of 8.5 atm; however, the influence of system pressure on liquid and solid chemical activity is generally small in the range of interest for heat pipe applications.

Chloride Working Fluids

On the basis of the decomposition potentials for chlorides presented in Figure 2.4-3, it can be generalized that working fluids are desired that have higher decomposition potentials than chlorides of the envelope material. For an aluminum envelope, most chloride fluids are seen to be of questionable character. On the other hand, there are a number of fluids that may be acceptable with iron or stainless heat pipes, including $TiCl_4$, $ZnCl_2$, $ZrCl_4$, $AlCl_3$, etc.

To gain a more intuitive perspective of this interesting class of fluids, Table 2.4-2 was generated to determine where on the periodic table chloride fluids can be found that are chemically compatible with standard materials and possess low melting points, since the chlorides as a ground have typically high melting points.

Chloride compounds of interest are found in groups 4b, 5b, and 3a, 4a, and 5a of the periodic chart. Of particular interest because of a low melting point and/or high decomposition potential at $25^{o}C$ are the compounds $AlCl_3$, $TiCl_4$, VCl_4, $NbCl_5$, $TaCl_5$, $ZnCl_2$, $GaCl_3$, $SnCl_2$, $SnCl_4$, $SbCl_3$, PCl_3, and $SbCl_3$.

TABLE 2.4-2. DECOMPOSITION POTENTIALS AND MELTING POINTS FOR CHLORIDE COMPOUNDS

1a	2a	3b	4b	5b	6b	7b	8	1b	2b	3a	4a	5a	6a	7a	0	Orbit
1 +1 H −1 – 605															2 0 He	K
3 +1 Li – 605	4 +2 Be – 405									5 +3 B 1.31 -107.3	6 +2 (+4) −4 C 0.18 -23.	7 +1 +2 +3 +4 +5 −1 −2 −3 N	8 −2 O	9 −1 F	10 0 Ne	K–L
11 +1 Na 3.98 801.	12 +2 Mg 3.07 714.	Transition Elements						Transition Elements		13 +3 Al 2.20 190	14 +2 (+4) −4 Si 1.48 -70.	15 +3 +5 −3 P .99 -112.	16 (+1) +4 +6 −2 S – -CC.	17 +1 +5 +7 −1 Cl	18 0 Ar	K–L–M
19 +1 K 4.23 770.	20 +2 Ca 3.89 782.	21 +3 Sc – 939.	22 +2 +3 (+4) Ti 1.75 -25.	23 +2 +3 (+4) +5 V – -28.	24 (+2) +3 +6 Cr 1.85 824.	25 (+2) +3 +4 +7 Mn 2.29 650	26 (+2) +3 Fe 1.57 672.	27 (+2) +3 Co 1.46 724.	28 (+2) +3 Ni 1.41 1001	29 (+1) +2 Cu 1.22 430.	30 +2 Zn 1.91 283.	31 +3 Ga – 77.9	32 +2 (+4) Ge – -49.5	33 (+3) +5 −3 As 1.02 -8.5	34 (+4) +6 −2 Se – 305.	35 +1 +5 −1 Br -66.	36 0 Kr	-L–M–N
37 +1 Rb 4.27 718.	38 +2 Sr 4.05 875.	39 +3 Y – 721.	40 +4 Zr 2.27 437	41 +3 (+5) Nb – 204.7	42 +6 Mo – d	43 +4 +6 +7 Tc – –	44 +3 Ru – >500d	45 +3 Rh – 450-500d	46 (+2) +4 Pd – 500d	47 +1 Ag 1.14 455.	48 +2 Cd 1.78 568.	49 +3 In – 586.	50 (+2) (+4) Sn 1.23/– 246./-33.	51 (+3) +5 −3 Sb 1.12 73.4	52 (+4) +6 −2 Te – 224.	53 +1 +5 +7 −1 I – 13.9	54 0 Xe	-M–N–O
55 +1 Cs 645.	56 +2 Ba 4.20 963.	57* +3 La – 860.	72 +4 Hf – 319S	73 +5 Ta – 216.	74 +6 W – 275.	75 (+4) +6 +7 Re – 500.	76 (+3) +4 Os – 500-600d	77 +3 +4 Ir – d	78 (+2) +4 Pt – 581d	79 (+1) +3 Au – 170d	80 +1 (+2) Hg 0.92 276.	81 +1 (+3) Tl – 430.	82 (+2) +4 Pb 1.63 501.	83 (+3) +5 Bi 1.10 231.	84 +2 (+4) Po – 300.	85 At	86 0 Rn	-N–O–P
87 +1 Fr	88 +2 Ra – 1000.	89** +3 Ac – 960s	104 —	105 —													O–P–Q

*Lanthanides	58 +3 +4 Ce – 848.	59 +3 Pr – 786	60 +3 Nd – 784	61 +3 Pm	62 +2 +3 Sm – d	63 +2 +3 Eu – 850.	64 +3 Gd – 609	65 +3 Tb	66 +3 Dy – 718.	67 +3 Ho – 718.	68 +3 Er	69 +3 Tm	70 +2 (+3) Yb – 865	71 +3 Lu – 905		N–O–P
**Actinides	90 +4 Th – 770.	91 +5 +4 Pa	92 +3 (+4) +5 +6 U 2.49 590.	93 +3 +4 +5 +6 Np	94 +3 +4 +5 +6 Pu	95 +3 +4 +5 +6 Am	96 +3 Cm	97 +3 +4 Bk	98 +3 Cf	99 Es	100 Fm	101 Md	102 No	103 Lr	104	O–P–Q

7706-232.7

2.5 Falling Film Erosion

Many metals show corrosion passivity as a result of a thin protective layer on the metal surface. With aluminum and titanium, for example, adherent oxide layers retard corrosion. Under typical use conditions, these oxide layers are rapidly established and maintained as a result of metal surface contact with atmospheric or dissolved oxygen. However, in many two-phase heat transfer systems such as heat pipes, it is not clear that an adequate supply of oxygen or other passivation agent will be available over the device operating life, and it would be useful to develop a model to predict the rate at which such passivation layers will be removed during device operation.

In the analysis presented here, dissolution of a sparingly soluble wall is modeled assuming laminar film condensation on a vertical surface in 1 g. This physical system was selected because it is very amenable to analysis and because a great number of heat transfer systems rely on vapor condensation on a vertical surface.

The condensing film and wall are shown in Figure 2.5-1 along with pertinent system variables. The z-axis is parallel to the direction of the film bulk flow, positive downward, with origin at the upper tip of the condensate film. The y-axis is perpendicular to the vertical wall with origin at the wall. The wall (species "a") is considered sparingly soluble such that the dissolution process does not influence film hydrodynamics significantly. The vapor phase in contact with the liquid is assumed pure, uniform in composition, uniform in temperature (T_{vs}), and of low density relative to the liquid phase. The liquid film is assumed to have invariant physical properties, and the wall upon which condensate forms is isothermal (T_w).

Flow Field Representation

Within the condensing film, it is assumed that flow is at most z- and y-directed, with flow velocities in the y-direction (U_y) being much smaller than flow velocities in the z-direction (U_z).

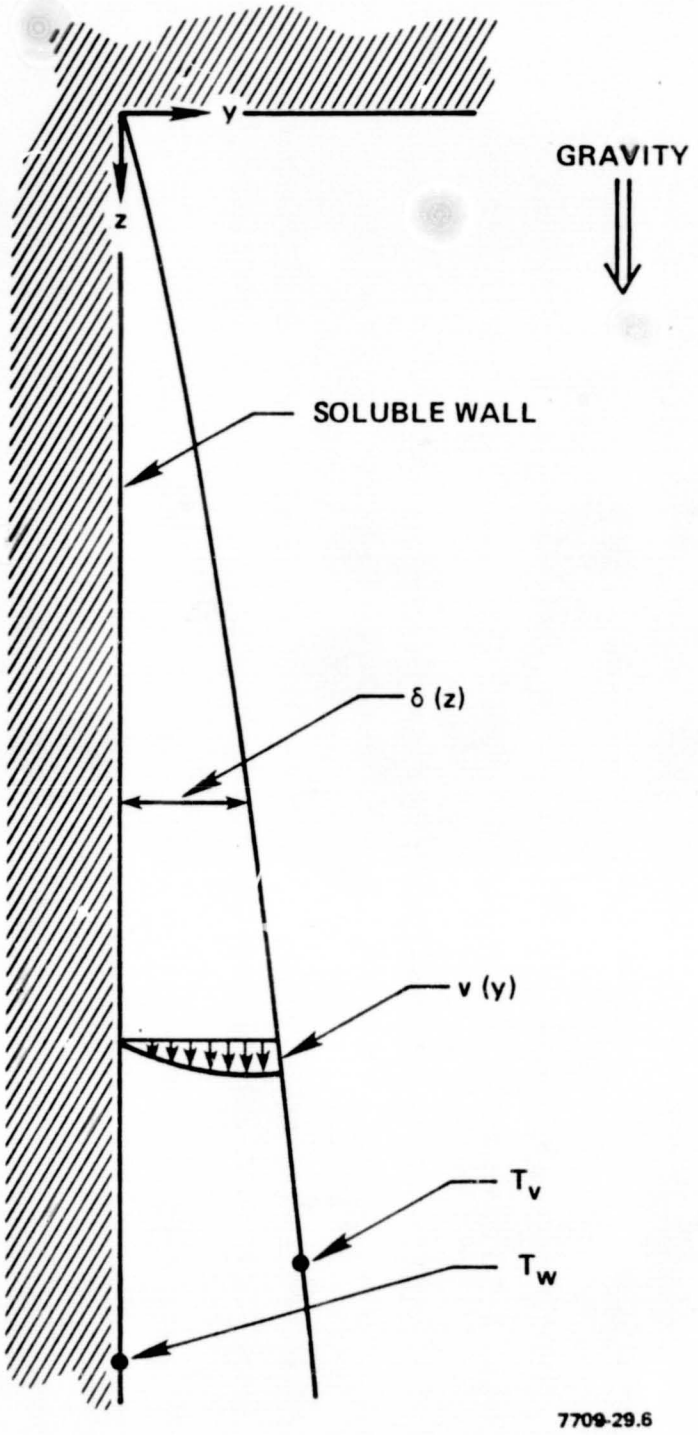

FIGURE 2.5-1. EROSION OF A VERTICAL WALL BY A CONDENSING NUSSELT FILM

Flow is governed by the y and z momentum equations and the equation of continuity,

$$U_z \frac{\partial U_z}{\partial z} + U_y \frac{\partial U_z}{\partial y} = - \frac{1}{\rho_b} \frac{\partial P_\ell}{\partial z} + \frac{\mu_b}{\rho_b} \left(\frac{\partial^2 U_z}{\partial z^2} + \frac{\partial^2 U_z}{\partial y^2} \right) + g \qquad (2.5\text{-}1)$$

$$U_z \frac{\partial U_y}{\partial z} + U_y \frac{\partial U_y}{\partial y} = - \frac{1}{\rho_b} \frac{\partial P_\ell}{\partial z} + \frac{\mu_b}{\rho_b} \left(\frac{\partial^2 U_y}{\partial z^2} + \frac{\partial^2 U_y}{\partial y^2} \right) \qquad (2.5\text{-}2)$$

$$\frac{\partial U_z}{\partial z} + \frac{\partial U_y}{\partial y} = 0 \qquad (2.5\text{-}3)$$

If the film is very thin, then $\partial P/\partial y$ can be considered negligible. In addition, if the vapor phase is assumed at a constant pressure, P_{vs} and the vapor-liquid interfacial resistance is small, then the pressure of the liquid, P_ℓ, is related to the vapor pressure by

$$P_\ell = P_{vs} + \frac{\sigma d^2\delta/dz^2}{\left[1 + \left(\frac{d\delta}{dz}\right)^2\right]^{3/2}} \qquad (2.5\text{-}4)$$

where σ is the surface tension and δ is the local film thickness. If the film thickness changes slowly, then the second term on the right side of equation (2.5-4) is small, and the liquid pressure is independent of both y and z.

The velocity U_y is expected to be much smaller than U_z and, hence, derivatives of U_y with respect to z, and products of U_y and its derivatives will also be small. The thin film also implies that $\partial U_z/\partial z$ is much smaller than $\partial U_z/\partial y$. When these boundary-layer assumptions are made, the equations (2.5-1) through (2.5-3) reduce to

$$U_z \frac{\partial U_z}{\partial z} + U_y \frac{\partial U_z}{\partial y} = \nu \frac{\partial^2 U_z}{\partial y^2} + g \qquad (2.5\text{-}5)$$

$$\frac{\partial U_z}{\partial z} + \frac{\partial U_y}{\partial y} = 0 \qquad (2.5\text{-}6)$$

where ν is the kinematic viscosity. To solve this set of equations, Nusselt assumed that the convective terms in equation (2.5-5) were small, so that

$$\frac{\partial^2 U_z}{\partial y^2} = - \frac{g}{\nu} \tag{2.5-7}$$

If vapor/liquid shear and interfacial condensation resistance are neglected, then the liquid film surface temperature T_δ is equal to the saturated vapor temperature, and

$$T_\delta = T_{vs} \qquad \left.\frac{\partial U_z}{\partial y}\right|_{y=\delta} = 0 \tag{2.5-8}$$

and the velocity U_z is found to be

$$U_z = \frac{\rho_b g \delta^2}{\mu_b} \left[\left(\frac{y}{\delta}\right) - \frac{1}{2} \left(\frac{y}{\delta}\right)^2 \right] \tag{2.5-9}$$

By substituting this velocity distribution into equation (2.5-6), the velocity U_y is found to be, for $U_y = 0$ at $y = 0$,

$$U_y = - \frac{\rho_b g \delta^2}{8\mu_b} \left(\frac{y}{z}\right) \left(\frac{y}{\delta}\right) \tag{2.5-10}$$

The film thickness δ is found by assuming a linear temperature profile across the film. Conservation of mass on a macroscopic level gives the film thickness δ as

$$\delta = \left(\frac{4\mu_b K_b (T_{vs} - T_w) z}{g \rho_b^2 h_{fg}} \right)^{1/4} \tag{2.5-11}$$

A derivation of the relation between film thickness and vertical position is given in Kreith.[34]

Wall Dissolution

Using the same boundary-layer arguments given in the previous section, the concentration of species "a" in the liquid "b" is governed by a z-directed diffusion equation analogous to equation (2.5-5).

$$U_z \frac{\partial C_a^+}{\partial z} + U_y \frac{\partial C_a^+}{\partial y} = D_{ab} \frac{\partial^2 C_a^+}{\partial y^2} \qquad (2.5\text{-}12)$$

where $C_a^+ = C_a/C_{as}$.

In the corresponding Nusselt analysis, the left-hand side of equation (2.5-12) was neglected. This is not physically realistic for mass transfer problems because the convective transport terms in equation (2.5-12) are of the same order of magnitude as the diffusive transport term. For laminar falling films of constant thickness, the velocity term U_y is set to zero in equation (2.5-12). In the present situation, however, the film actually grows slowly in thickness (as $z^{1/4}$), and the convective term $U_y\ \partial C_a^+/\partial y$ may be of some importance. In the following analysis this term was retained, and a comparison of erosion rates is made at a later point with a solution in which the term $U_y\ \partial C_a/\partial y$ was neglected.

It is assumed that $y = 0$, the liquid film is saturated with species "a" at concentration C_{as}. If the equation (2.5-12) is assumed to have a similarity solution with similarity variable $\eta = y/\delta$, the equation (2.5-12) is transformed to the ordinary second-order differential equation

$$C_a^+ = f(\eta) : \eta = y/\delta \qquad (2.5\text{-}13a)$$

$$-\frac{\theta}{2}(3\eta^2 - \eta^3)\frac{dC_a^+}{d\eta} = \frac{d^2C_a^+}{d\eta^2} \qquad (2.5\text{-}13b)$$

where $\theta = \dfrac{K_b\ (T_{vs} - T_w)}{\rho_b\ D_{ab}\ h^\circ_{fg}}$. (2.5-13c)

Use has been made of U_y and U_z given respectively by equations (2.5-10) and (2.5-9) of the Nusselt analysis. If equation (2.5-13b) is integrated twice, with $C_a^+ = 1$ at $\eta = 0$, the concentration profile is given by

$$C_a^+ = 1 + A\int_0^{\eta} \text{EXP}\left[-\frac{\theta x^3}{2}\left(1 - \frac{x}{4}\right)\right]dx \qquad (2.5\text{-}14)$$

where A is a constant that remains to be identified. The constant A can be found by at least two different methods. In the first method, conservation of species "a" on a macroscopic slice of film yields an equality between the integrated diffusive flux at $y = 0$ from $0 \leq z \leq L$ and the z-directed convective flux across the arbitrary lower boundary $z = L$. In the second method, a careful analysis of the film/vapor boundary yields a relation between C_a^+ and $dC_a^+/d\eta$, from which A can be found. Both methods yield the same numerical value for A, although the mathematical formulations are quite different in appearance.

The first derivation is somewhat lengthy, although straightforward, and will not be detailed here. The constant A is found by this solute-conservation approach to be

$$A = -\theta/[1 + \theta(F_0 - \tfrac{3}{2}F_2 + \tfrac{1}{2}F_3)] \qquad (2.5\text{-}15)$$

where the F_N are defined by

$$F_N = \int_0^1 x^N \cdot \text{EXP}\left[-\frac{\theta x^3}{2}\left(1 - \frac{x}{4}\right)\right]dx \qquad (2.5\text{-}16)$$

In the second approach, the condensation process is considered for a small triangular section, as in Figure 2.5-2. Over the height Δz, the film thickness increases an amount of $\Delta\delta$ from the condensation flux $\dot{m}$ onto the existing surface. At steady state, the convective and diffusive fluxes into this wedge-shaped element must sum to zero:

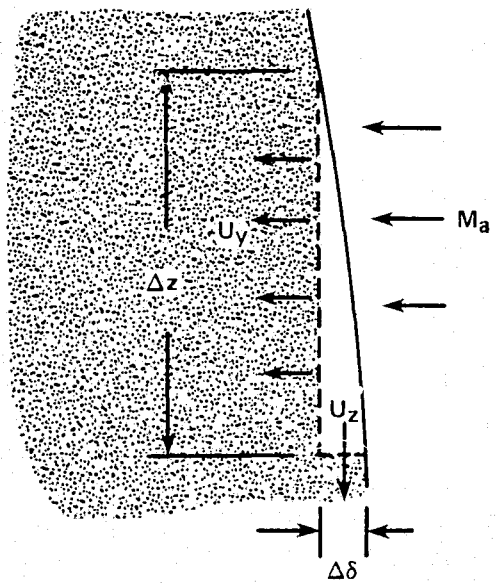

FIGURE 2.5-2. SOLUTE CONSERVATION AT THE OUTER GROWING FILM SURFACE REQUIRES THAT THE y-DIRECTED CONVECTIVE AND DIFFUSIVE FLUX EQUALS THE z-DIRECTED CONVECTIVE FLUX.

7706-232.3

$$\Delta z \cdot \left(C_a^+ U_y - D_{ab} \frac{\partial C^+}{\partial y} \right) \Bigg|_{y=\delta} = C_a^+ U_z \Delta\delta \Big|_{y=\delta} \qquad (2.5\text{-}17)$$

For Δz vanishingly small, this leads to

$$C_a^+ = \frac{- D}{\left(U_z \frac{d\delta}{dz} - U_y \right)} \cdot \frac{\partial C_a^+}{\partial y} \qquad (y = \delta) \qquad (2.5\text{-}18)$$

When this is transformed into a similarity solution boundary condition, the equation (2.5-18) becomes

$$C_a^+ = - \frac{1}{\theta} \frac{dC_a^+}{d\eta} \qquad (\eta = 1) \qquad (2.5\text{-}19)$$

When boundary condition (2.5-19) is applied to the solution equation (2.5-14), the constant A is bound to be

$$A = \frac{- 1}{F_0 + \frac{1}{\theta} \text{EXP} \left(- \frac{3}{8} \theta \right)} \qquad (2.5\text{-}20)$$

and the concentration C^+ is

$$C_a^+(\eta) = \frac{1 + B \cdot [1(1) \cdot 1(\eta)]}{1 + B \cdot 1(1)} \qquad (2.5\text{-}21)$$

where

$$1(\eta) = \int_0^{\eta} \text{EXP} \left[- \frac{\theta x^3}{2} \left(1 - \frac{x}{4} \right) \right] dx \qquad (2.5\text{-}22)$$

If the solution (2.5-21) is used to calculate the erosion rate, the average diffusive flux density ϕ_L at the surface y = 0 is found to be

$$\bar{\phi}_L = \frac{C_{as} D_{ab}}{\delta(L)} \cdot g(\theta) \qquad (\text{cm}^{-2} \text{ sec}^{-1}) \qquad (2.5\text{-}23)$$

where the flux density has been averaged over the vertical range $0 \leq z \leq L$. The function $g(\theta)$ is given in Table 2.5-1 for $0.001 \leq \theta \leq 100$.

This range covers most heat pipe fluids and heat flux densities. The concentration of species "a" at the free surface of the condensing film is also tabulated.

The factor $g(\theta)$ is also given in Figure 2.5-3. In this figure, $g(\theta)$ is shown both as curve (1) for the case in which the y-directed velocity is included in the governing equation (2.5-12), as well as by curve (2) for the case in which U_y is assumed negligible. For small values of the parameter θ, the two solutions are indistinguishable. Above $\theta = 1.0$, curve (1) predicts a diffusive erosion rate about 15 to 20% higher than curve (2).

When the various factors in equation (2.5-23) are related to an average heat flux density, $Q_{a\ell}$, it is found for $\theta < 0.4$ that the erosion rate is approximately proportional to the solute saturated concentration C_{as} and the average condensing mass flux per unit area. At high heat flux densities ($\theta > 2$), the film is thick compared to the penetration depth of the solute, so that the dependence on heat flux density is small and the erosion rate varies as the 0.64 power of D_{ab}. The importance of C_{as} is undiminished at large θ.

As a specific example, consider at $20^{o}C$ a condensing ammonia system with a saturated vapor to wall temperature difference of $1.0^{o}C$. For a vertical film 10 cm in height, the maximum film thickness is 5.07 (10^{-3}) cm. If the wall is covered with a layer of hydrated aluminum oxide, then it may be possible for this layer to be slowly dissolved by the condensing ammonia and ultimately allow direct contact of the ammonia solution with the base metal. If the maximum allowable surface loss is, for example, 0.01 cm per year, then the previous equations can be used to calculate the maximum permissible solubility (C_{as}) of the hydrated alumina in ammonia.

In aqueous solution, the mean diffusivity of aluminum and hydroxide ions is about 1.5 (10^{-5}) $cm^2/sec.$, and their diffusivities in ammonia will be comparable or larger because of the much lower viscosity of ammonia. However, if the

TABLE 2.5-1. DIMENSIONLESS DERIVATIVE FACTOR FOR CONDENSING FILM DISSOLUTION

θ	Derivative Factor, $g(\theta)$	$C_{a\delta}/C_{as}$
0.001	0.00133	0.9990
0.002	0.00266	0.9980
0.005	0.00665	0.9950
0.010	0.01325	0.9901
0.020	0.02634	0.9803
0.050	0.06465	0.9518
0.10	0.1255	0.9068
0.20	0.2373	0.8255
0.40	0.4283	0.6911
0.60	0.5862	0.5851
0.80	0.7197	0.4999
1.00	0.8347	0.4303
2.00	1.242	0.2201
4.00	1.703	0.07124
6.00	1.997	0.02630
8.00	2.221	0.01037
10.00	2.408	0.00425
20.00	3.077	0.00006
40.00	3.917	$<1(10^{-5})$
60.00	4.505	$<1(10^{-5})$
80.00	4.083	$<1(10^{-5})$
100.00	5.368	$<1(10^{-5})$

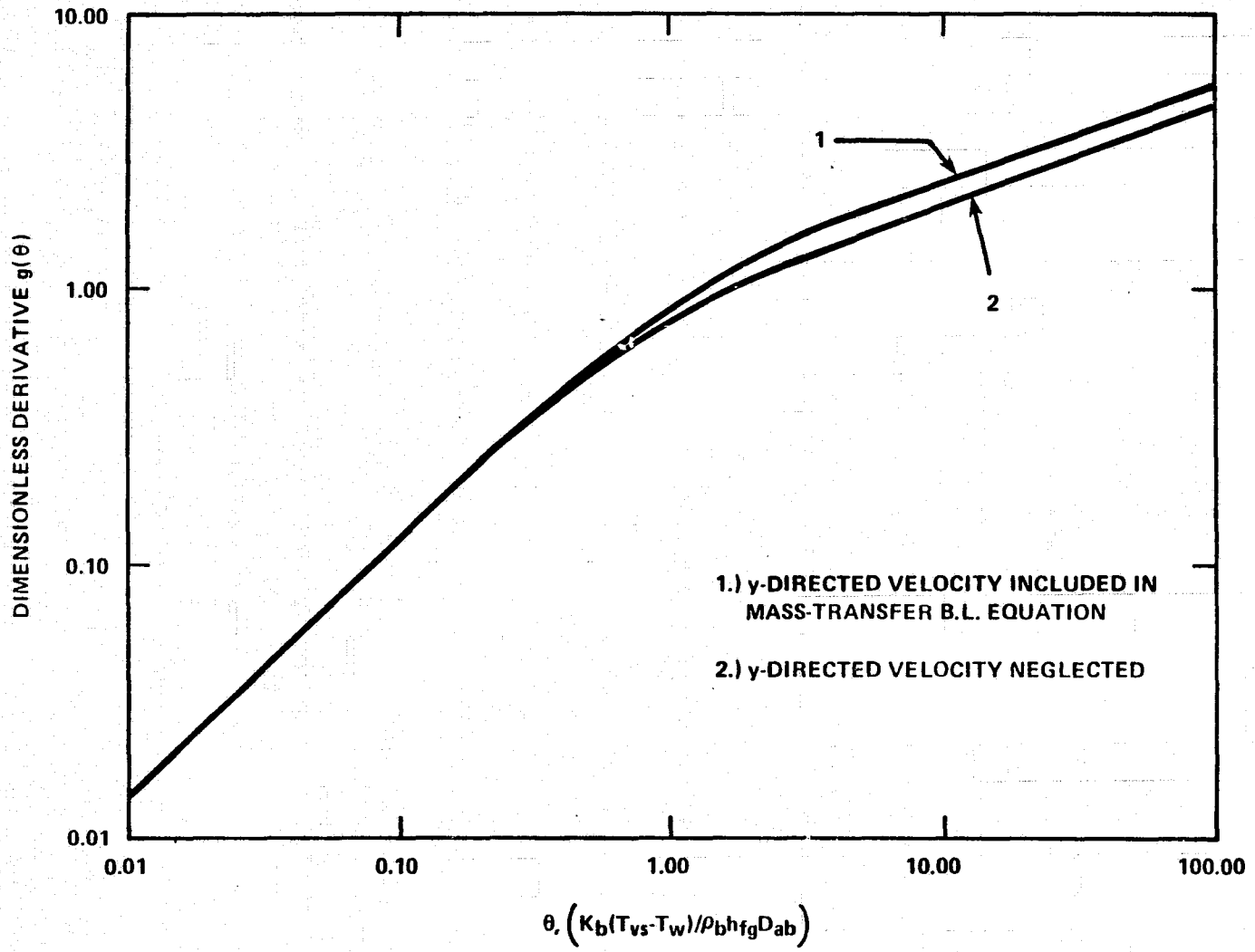

FIGURE 2.5-3. THE DIMENSIONLESS DERIVATIVE FACTOR g(θ) VERSUS THE DIMENSIONLESS FACTOR θ. THE DEPENDENCE g(θ) ESTABLISHES THE INFLUENCE OF FLUID PROPERTIES AND THE DRIVING TEMPERATURE DIFFERENCE ON WALL EROSION.

7706-232.2

value D_{ab} = 1.5 (10^{-5}) cm^2/sec is also used for ammonia, then the factor θ is about 0.455, and $g(\theta)$ = .47. If the surface is composed of boehmite ($Al_2O_3 \cdot H_2O$), then a loss of 0.01 cm per year corresponds to a solubility of 1.15 (10^{-11}) g-moles/liter, and a solubility product $[(Al^{-3})(OH^-)^3]$ of 4.7 (10^{-43}). In water, Pourbaix[35] indicates that the solubility product of boehmite is 10^{-34}, or a factor of 10^8 larger. This implies that the solubility product for $Al_2O_3 \cdot H_2O$ in ammonia can be a factor of 10^8 less than the measured value in water, yet results in a surface loss rate of about 0.01 cm per year. These calculations indicate that in refluxing systems, even a very small solubility of the wall material in the working fluid can lead to a significant surface loss rate over a period of several months or years. This mass loss can expose a base metal to corrosion, lead to noncondensable gas generation, or cause capillary pore clogging in the evaporator zone.

3.0 EXPERIMENTAL TEST EQUIPMENT

Heat Pipe Description

The heat pipes used in reflux compatibility tests were of the design shown in Figure 3-1. The reflux capsules were constructed of A-178 carbon steel and 6061 aluminum. This particular steel was selected on the basis of widespread national use in boilers, sheet and tube heat exchangers, and other heat transfer equipment. The aluminum alloy 6061 was selected because it is used extensively for aerospace heat pipe applications where low weight and high strength are desirable.

The active heat pipe length was 44.5 cm and the heat pipe internal diameter was 1.26 cm. Evaporator length was 15.25 cm, adiabatic length was 15.25 cm, and the condenser length was 14 cm. In operation, the evaporator and adiabatic sections were surrounded by an insulation shell consisting of multiple wraps of a high temperature insulating ceramic felt (Cerafelt$_{TM}$) with an outside insulation package diameter of 7.6 cm. This insulation package in turn was inserted into a thin cylindrical aluminum shell, while the condenser was in direct contact with laboratory ambient.

For both the aluminum and steel heat pipes, a single layer of square-weave screen was used in the evaporator. In the aluminum capsules, the screen was 100 mesh 1100 alloy aluminum, while in the steel capsules, 200 mesh 304 stainless steel was used. The function of the screen was to uniformly distribute the fluid around the circumference to preclude thin-film evaporative instabilities. In addition, as with any heat pipe, evaporation will concentrate any dissolved species picked up from the condenser or adiabatic, and clogging of the screen can be evaluated through subsequent metallurgical examination. The adiabatic and condenser inner surfaces were not screen-covered, to obtain as clear and unequivocal a picture as possible of erosion phenomena.

A summary of heat pipe characteristics is given in Table 3-1.

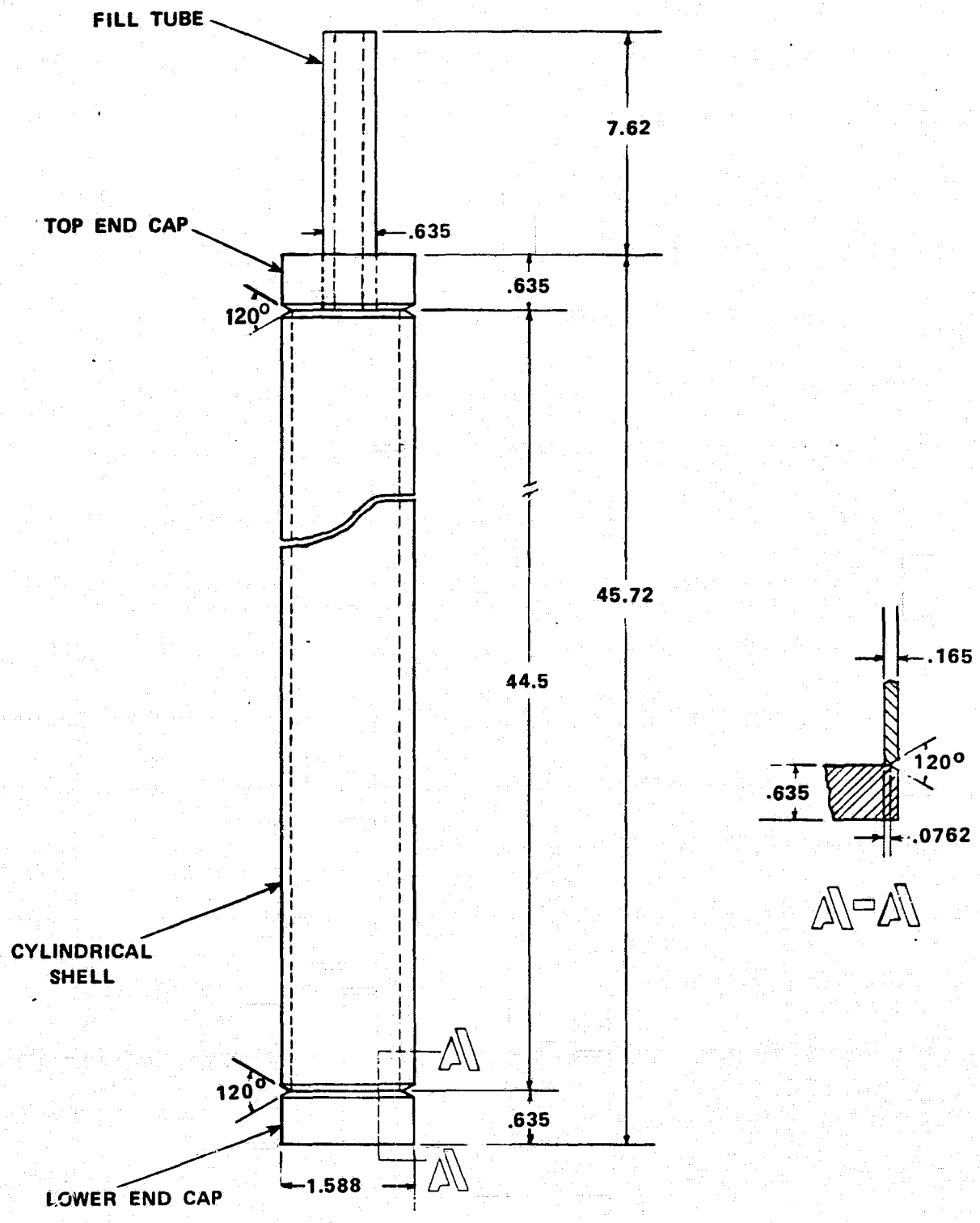

FIGURE 3-1. CAPSULE DESIGN FOR HEAT PIPE FLUID COMPATABILITY STUDIES. DRAWING TAKEN FROM BLUEPRINTS.

7706-232.12

TABLE 3-1. HEAT PIPE DESIGN SUMMARY

Parameter	Value	
	Aluminum	Steel
Material	6061	A-178
Physical dimensions		
Diameter (I.D./O.D.), cm	1.26/1.588	1.26/1.588
Evaporator length, cm	15.25	15.25
Adiabatic length, cm	15.25	15.25
Condenser length, cm	15.0	14.0
Wicking (evaporator only)	100 mesh, 1100 series alloy	200 mesh, 304 stainless alloy

Heaters

The heaters are tight-fitting cylindrical steel shells with a 0.10 cm O.D. stainless sheathed heater wire brazed to the outer shell diameter (Figure 3-2). The sheathed heater wires have not been brazed or soldered directly to the heat pipes to simplify heater replacement in case of failure, and to preclude diffusion of the braze or solder constituents through the heat pipe wall. The heater shells incorporate an axial slot and a tensioning mechanism to maintain adequate contact with the heat pipe. In addition, the heat pipes are coated with a heat transfer cement prior to heater attachment. The cement binder volatilizes at a low temperature, leaving a ceramic powder that aids heat transfer and allows the heater to be removed with minimal effort at a later time. Several heater failures during test were found to result from oxidation of 14 gauge multistrand asbestos-covered copper lead-in wires. This problem was corrected with the substitution of 0.16 cm diameter stainless steel lead-in wires in the high temperature evaporator zone.

Cleaning Procedure

Cleaning procedures were used to render the surfaces oil-free and devoid of particulate matter, but no attempt was made to passivate the surfaces. The procedures used are summarized in Table 3-2.

Fluid Charging

Each heat pipe was charged such that at a maximum operating pressure of 10 atmospheres, a liquid pool of approximately 1.3 cm depth would be present. To calculate the fluid charge, the wick was assumed completely saturated, and the adiabatic and condenser sections covered by a laminar Nusselt film. A heat flux of 50 watts was assumed. The fraction of total charge needed for the vapor phase was generally small, and operation at a lower vapor pressure would not appreciably increase the liquid pool height.

The organic working fluids were loaded in air, and the heat pipes sealed with a Swagelok$_{TM}$ cap . The hygroscopic inorganic fluids were loaded in

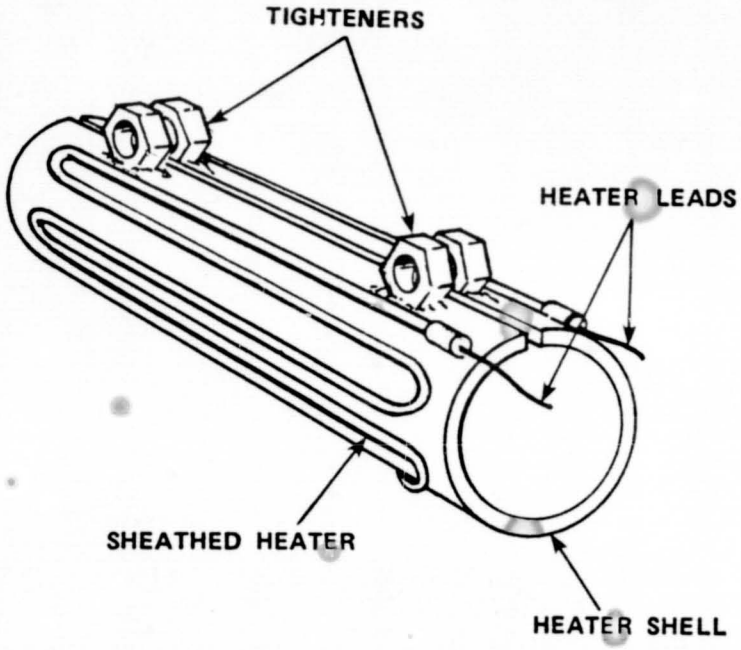

FIGURE 3-2. COMPLETED HEATER ASSEMBLY FOR USE WITH HIGH TEMPERATURE COMPATIBILITY TESTS. SHEATHED HEATER 'S SILVER-SOLDER BONDED TO HEATER SHELL.

7706-232.13

TABLE 3-2. HEAT PIPE CLEANING PROCEDURES

Capsules

1. Clean with Alconox$_{TM}$ and water
2. Rinse with water
3. Rinse with isopropyl alcohol
4. Dry and cap

Screen Wick

1. Ultrasonically clean 5 minutes in acetone
2. Rinse with clean acetone
3. Ultrasonically clean 5 minutes in isopropyl alcohol
4. Dry with hot air

a dry nitrogen glove box and fitted with stainless bellows valves. The resulting noncondensable gas charges were removed by operating the heat pipes slightly above a vapor pressure of 1 atmosphere, and discharging the gas/vapor mixture until the condenser was uniform in temperature.

Test Station

For this program, a special testing station was constructed, incorporating individual variable-voltage autotransformers for each heat pipe, as well as an overhead fume hood (Figure 3-3). Both the autotransformers and a $0.1^{o}C$ resolution Doric Digitrend data acquisition system have been operated from isolation transformers to eliminate early experimental difficulties with ground currents.

During operation, heat pipe function has been monitored using three special-limit type K thermocouples per heat pipe. These temperatures are measured on the outer wall at the centers of the evaporator and adiabatic sections, and at the far end of the condenser section.

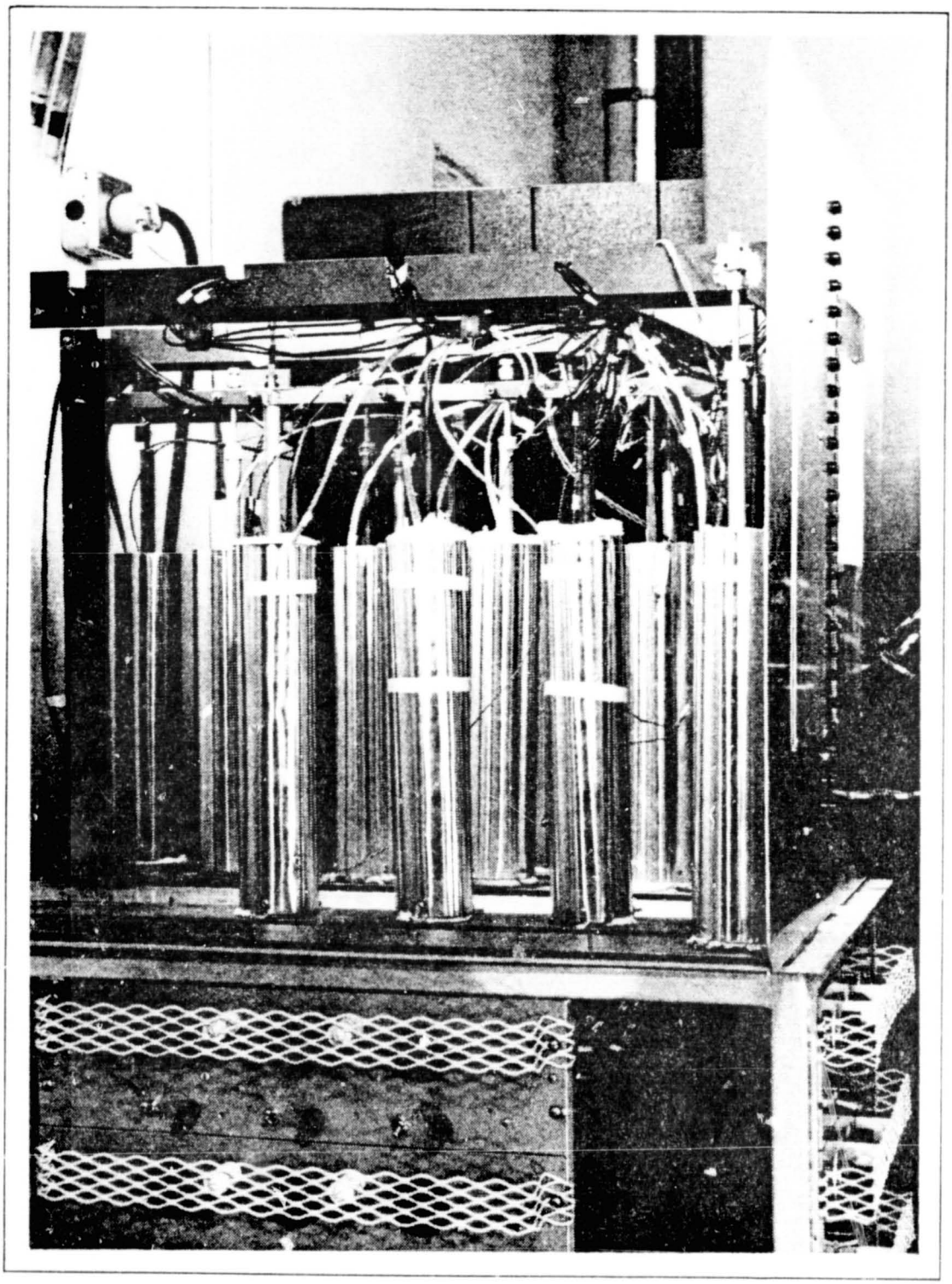

FIGURE 3-3. REFLUX HEAT PIPES AND TEST STAND

7706-232.1

4.0 COMPATIBILITY TESTS

Ten working fluids have been installed in mild steel (A-178) and aluminum (6061) reflux capsules, as described in Section 3.0.

The working fluids selected represent aromatic hydrocarbons (toluene, napthalene, biphenyl and o-terphenyl), halogenated aromatic hydrocarbons (monochloronapthalene and 1-fluoronapthalene), and inorganic molecular fluids (carbon disulphide, tin tetrachloride, titanium tetrachloride, and antimony trichloride). The working fluids were all reagent-grade materials with the exception of monochloronapthalene, which is of undetermined purity. The various fluids have been in test for varying periods of time up to 3500 hours. Operating temperatures have been selected so that the capsules are generally at the normal boiling point or 1-2 atmospheres above the boiling point. Table 4-1 shows the evaporator and condenser temperature drops ΔT_{ea} and ΔT_{ac} at test initiation and at the present time (June 1977). The evaporator-adiabatic temperature difference ΔT_{ea} provides an operational indicator of any changes in the evaporative surface or wicking that might influence evaporative heat transfer. Correspondingly, the adiabatic-condenser temperature difference ΔT_{ac}, is an accurate measure of noncondensable gas build-up. In an experimental scheme such as the one used here, where heat is directly rejected to laboratory ambient, variations in air temperature can cause some fluctuations in ΔT_{ac}, and variations of $\pm$ 1°C were not uncommon.

Of the 18 permutations tested, three working fluid/container combinations were found to be totally incompatible at test temperature, and a fourth combination is suspect, although testing time was not adequate because of a heater failure. For the 14 that were found to be useable, the evaporator-adiabatic temperature difference ΔT_{ea} was found not to vary significantly over the life test period. The adiabatic-condenser temperature differences, however, differed considerably from combination to combination. As mentioned earlier, this temperature difference is an indication of the amount of noncondensable gas generated during reflux operation. Table 4-2 summarizes operation of eleven combinations that showed consistently low values of ΔT_{ac}, or showed significant reductions in ΔT_{ac}. The remaining three combinations showed moderate increases in ΔT_{ac}, and

TABLE 4-1
CORROSION SUMMARY

Working Fluid (Boiling point, ^{o}C)	Envelope[1]	Operating Time (Hr)	Operating Temperature (^{o}C)	Heat Input (Watts)	ΔT_{ea}[2] (init./final) (^{o}C)	ΔT_{ac}[2] (init./final) (^{o}C)
carbon disulphide (46.5^{o})	Al	0/2014/3570	59	7.05	0.43/0.43/.33	0.68/0.86/1.03
	C.S.	0/2014/3570	60	6.4	0.33/0.33/.23	0.10/0.10/0.10
toluene (110.4^{o})	Al	0/2014/3570	130	26.2	2.53/2.80/3.1	2.53/2.94/1.9
	C.S.	0/672	119	26.0	1.72/1.56	3.36/4.86
tin tetrachloride (114.1^{o})	Al	-	159	INCOMPATIBLE		
	C.S.	0/2014/3570	159	26.0	1.24/3.3/3.4	1.54/10.6/11.5
titanium tetrachloride (136.4^{o})	Al	0/664/2210	165	29.6	5.67/5.7/6.5	1.63/8.65/11.3
	C.S.	0/2014/3570	152	38.8	2.60/4.25/4.5	1.70/1.7/1.5
1-fluoronapthalene (216.0^{o})	C.S.	0/656/2200	263	74.7	7.00/7.00/7.00	4.78/5.2/5.0
napthalene (217.9^{o})	Al	0/2014/3570	218	52.5	10.7/11.7/11.3	4.50/4.1/3.5
	C.S.	0/2014/3570	217	65.0	2.9/3.23/3.1	3.30/2.9/2.6
antimony trichloride (219.0^{o})	Al	-	227	INCOMPATIBLE		
	C.S.	0/1518/3060	227	41.5	6.23/5.7/6.2	95.6/77.0/61.1
monochloronapthalene (250^{o})	C.S.	0/642	266→306	INCOMPATIBLE		
biphenyl (255^{o})	Al	0/2014	275	63.7	9.9/10.3	3.48/10.0
	C.S.	0/1675	267	89.3	5.80/5.4	3.72/3.80
O-terphenyl (332^{o})	Al	0/672	290→308	77.8	7.20/8.3	47.6/87.2
	C.S.	0/2014/3570	283	71.7	9.17/9.50/9.4	52.8/55.8/42.7

[1] Al = 6061 aluminum, C.S. = A-178 carbon steel

[2] ea = evaporator-adiabatic temperature difference; ac = adiabatic-condenser temperature difference

TABLE 4-2. TWO-PHASE FLUID/ENVELOPE COMBINATIONS SHOWING LOW NONCONDENSABLE GAS GENERATION RATES

Working Fluid	Envelope	Operating Time (hr)	Operating Temperature (°C)
carbon disulphide	Al	3570	59
	C.S.	3570	60
toluene	Al	3570	130
	C.S.	672	119
titanium tetrachloride	C.S.	3570	152
1-fluoronapthalene	C.S.	2200	263
napthalene	Al	3570	218
	C.S.	3570	217
biphenyl	C.S.	1675	267
antimony trichloride	C.S.	3060	227
O-terphenyl	C.S.	3570	283

are noted in Table 4-3 and Figure 4-1. Figure 4-1 also presents historical data for monochloronapthalene/steel, o-terphenyl/aluminum, and antimony trichloride/steel.

It can be seen that the time dependence of ΔT_{ac} is significantly different for the various working fluids and metal envelopes. In the case of antimony trichloride/steel (227^{o}) and O-terphenyl/steel (283^{o}), ΔT_{ac} falls with time, indicating a reduction in NCG, while for titanium tetrachloride/aluminum (165^{o}) and tin tetrachloride/steel (159^{o}), ΔT_{ac} shows an increase with time. This divergent behavior may be caused by competing decomposition and permeation loss mechanisms. It is quite probable that the noncondensable gas being generated in both the inorganic and organic-charged heat pipes is hydrogen. In organic heat pipes, hydrogen could be generated through pyrolysis or polymerization of the working fluid or various impurities, while in inorganic heat pipes, hydrogen might be produced by trace quantities of water reacting with the reflux capsule wall. In these tests, water contamination is particularly probable because of the hydroscopic nature of the metal halide working fluids. Molecular hydrogen is soluble in most metals, and it is possible to lose this noncondensable gas by diffusion through the reflux capsule wall. It is well known, for example, that steel is relatively permeable to hydrogen, and that the permeability is exponential in temperature. Therefore, systems operating at lower temperatures might be expected to accumulate NCG because of a low wall permeability, while systems at high temperature would be more capable of losing accumulated hydrogen gas through permeation. Aluminum and aluminum oxide both have low hydrogen solubilities, and on this basis, aluminum reflux capsules would be expected to retain hydrogen gas to a greater extent than steel capsules. This was found to be true in at least one case. The o-terphenyl/aluminum combination operated at $290^{o}C$ did not show a reduction in ΔT_{ac} with time.

Both tin tetrachloride/steel ($159^{o}C$) and monochloronapthalene/steel ($257^{o}C$) have shown a period of initially slow NCG build-up that persists for several hundred hours, followed by a sudden rapid increase in NCG content (Figure 4-1). This unusual behavior is, in part, caused by the fact that as NCG builds up at a constant heat input, the available condenser area is reduced and the reaction rate increases exponentially with the increasing reflux capsule temperature. This is not a totally satisfactory explanation for this behavior, however,

TABLE 4-3 TWO-PHASE FLUID/ENVELOPE COMBINATIONS SHOWING MODERATE NONCONDENSABLE GAS GENERATION RATES

Working Fluid	Envelope	Operating Time (hr)	Operating Temperature (^{o}C)
tin tetrachloride	C.S.	3570	159
titanium tetrachloride	Al	2210	165
biphenyl	Al	2014	275

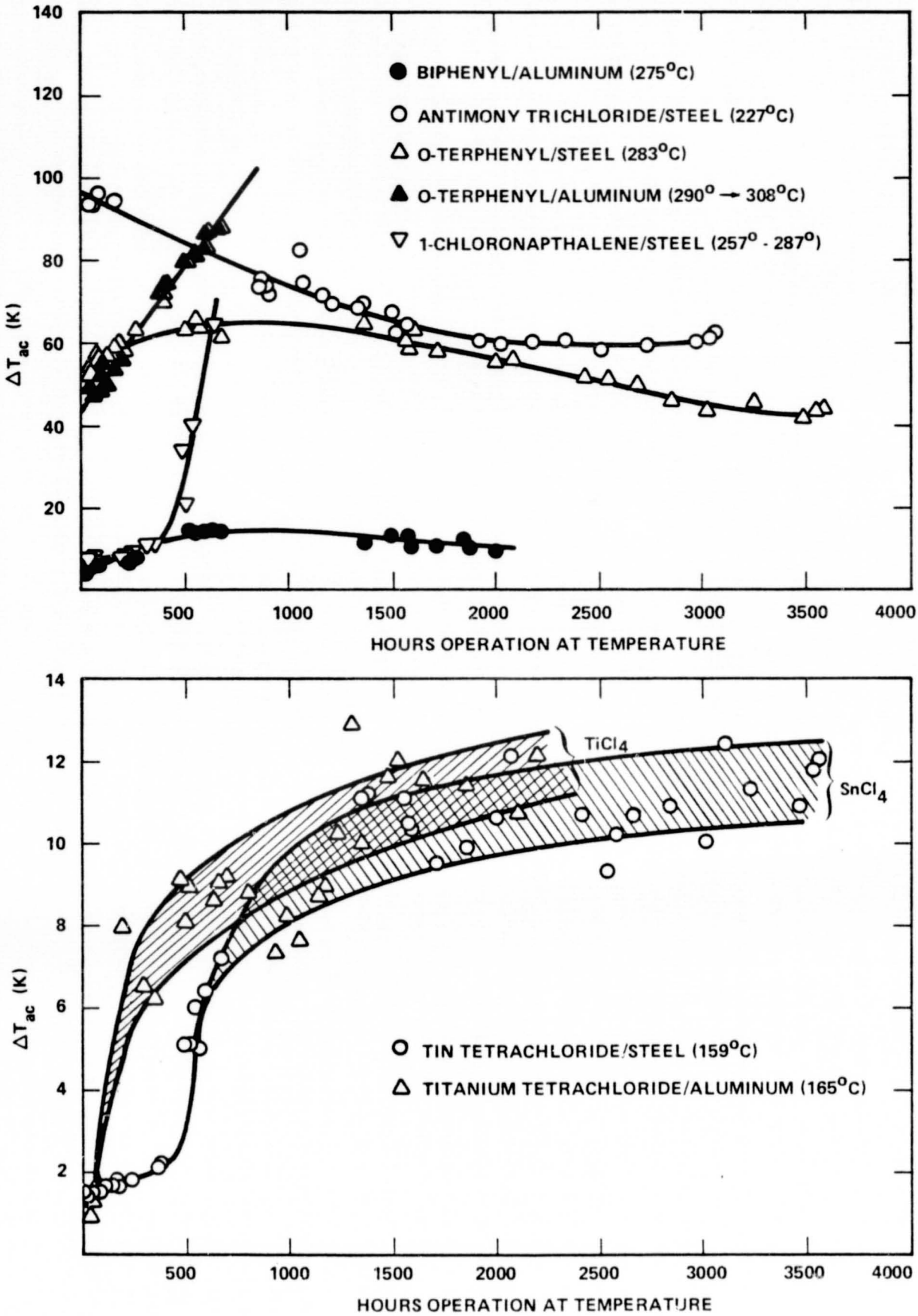

FIGURE 4.1. REPRESENTATIVE ADIABATIC-CONDENSER TEMPERATURE DIFFERENCES FOR REFLUX CAPSULES THAT GENERATED SIGNIFICANT AMOUNTS OF NONCONDENSABLE GAS

since the increase in temperature of the tin tetrachloride/steel capsule was relatively modest. It is also possible that these latency periods are connected to a surface erosion phenomena as discussed in Section 2.5, and that the initial passivity represents the time needed to erode a protective surface layer of oxide.

Of the various combinations tested, three were found unsatisfactory; tin tetrachloride/aluminum at 159°C, antimony trichloride/aluminum at 227°C, and monochloronapthalene/steel at 266°C. On the basis of the decomposition potentials of Figure 2.4-3, both tin tetrachloride/aluminum and antimony trichloride/aluminum would be expected to be unstable combinations. In addition to these three combinations, O-terphenyl/aluminum at 290°C may also be unsatisfactory, although a premature heater failure did not allow long-term operation.

In the case of tin tetrachloride, the heat pipe operated satisfactorily for a short time, and then displayed a nonrecoverable burn-out (that is, the evaporator would rise rapidly in temperature with small heat inputs). Upon sectioning, the heat pipe was found to contain a layer of metallic tin plated onto the heat pipe inside diameter, and a solid plug of tin in the far end of the evaporator (Figure 4-2). Upon prolonged contact with air, the layer of tin separated from the heat pipe wall to produce the exfoliated structure shown in Figure 4-2.

The antimony trichloride/aluminum combination showed initially a large noncondensable gas leg that increased with time. Upon sectioning, the heat pipe wick was found to be partially decomposed, with both amorphous and crystalline deposits of antimony on the heat pipe wall (Figure 4-3). For both metal halides, it appears that the greater thermodynamic stability of aluminum trichloride allowed decomposition of the working fluid to form the corresponding halide metal. Aluminum trichloride has a melting point of 190°C at a pressure of 2.5 atmosphere, and a vapor pressure of 1 atmosphere at 183°C. Therefore, at 159°C, the vapor pressure of aluminum trichloride is considerably less than the vapor pressure of tin tetrachloride (3.2 atm), and it would be expected that the primary mode of failure at this temperature would be the creation of solid phases that inhibited evaporative heat transfer, as was found. At 227°C, however, aluminum trichloride is a liquid and has a vapor pressure of about 5.4 atm, whereas antimony trichloride has a vapor pressure of 1.15 atmosphere. Under these conditions, aluminum trichloride would behave as a noncondensable gas, as was observed experimentally.

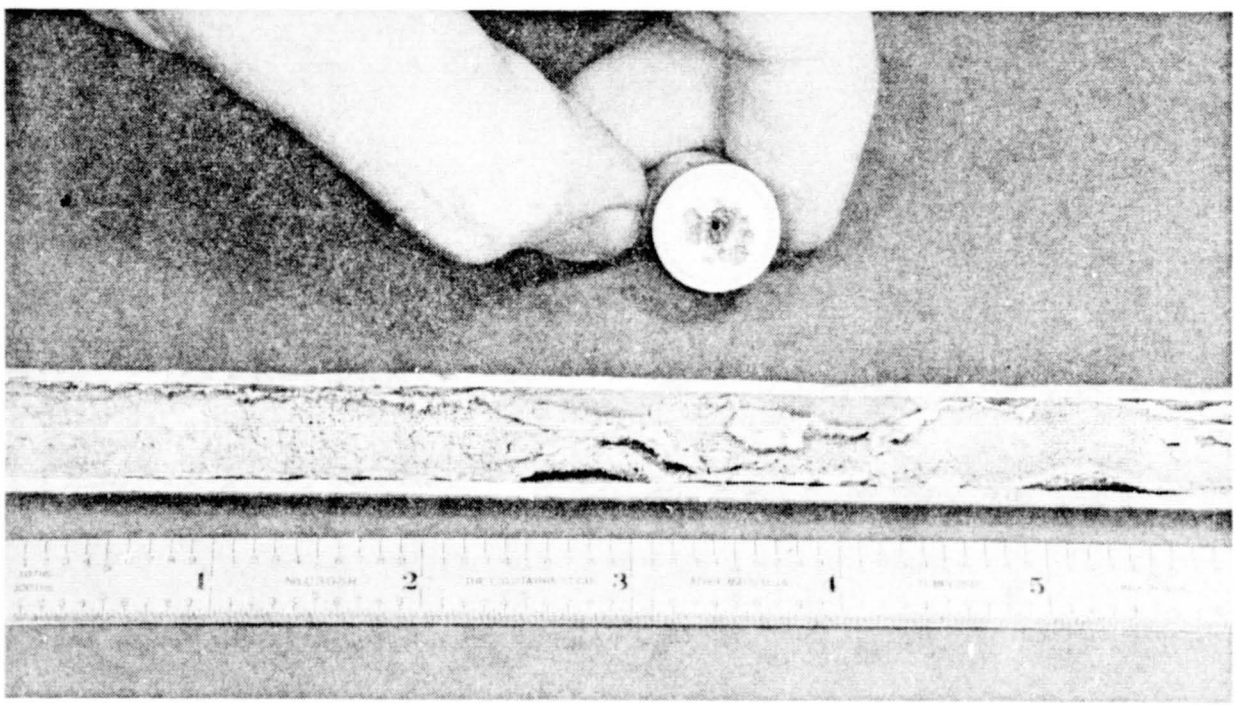

FIGURE 4-2. LONGITUDINAL AND TRANSVERSE VIEWS OF TIN TETRACHLORIDE/ALUMINUM REFLUX CAPSULE AFTER FAILURE AT 159°C. EXFOLIATED STRUCTURE IS A LAYER OF METALLIC TIN. UPON FAILURE, REFLUX CAPSULE TEMPERATURE EXCEEDED THE MELTING POINT OF TIN, PRODUCING THE PLUG OF SOLID METAL IN THE BLIND END OF THE EVAPORATOR, AS SHOWN. THERMODYNAMIC CALCULATIONS PREDICT THIS COMBINATION OF FLUID AND ENVELOPE TO BE UNSTABLE.

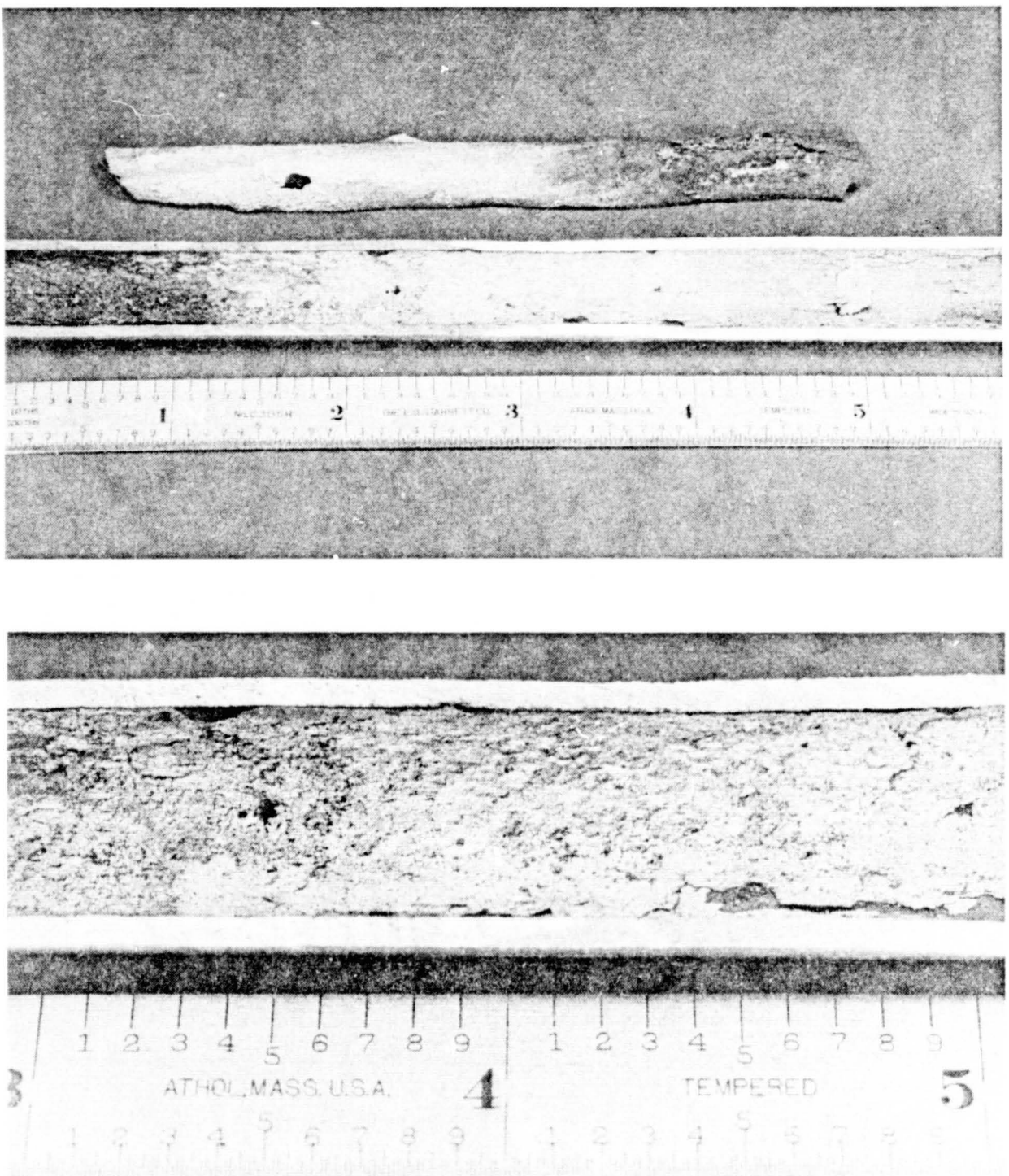

FIGURE 4-3. LONGITUDINAL VIEWS OF ANTIMONY TRICHLORIDE/ALUMINUM REFLUX CAPSULE EVAPORATOR AFTER FAILURE AT 227°C. THE 100 MESH ALUMINUM SCREEN WICK WAS BADLY CORRODED, WITH EXTENSIVE DEPOSITS OF BOTH AMORPHOUS AND CRYSTALLINE ANTIMONY ON THE CAPSULE INNER WALL. THERMODYNAMIC CALCULATIONS PREDICT THIS COMBINATION OF FLUID AND ENVELOPE TO BE UNSTABLE.

Monochloronapthalene/steel at 266°C produced large quantities of noncondensable gas. Upon heat pipe sectioning, minimal deterioration of either the wall or wick was found, although there were deposits of an unidentified sludge in the evaporator (Figure 4-4). The working fluid had changed from a colorless mobile liquid to a dark viscous oil. Chemical analysis established the presence of free chloride and ferric ions in the working fluid, indicating that the steel wall participated in the stripping of chlorine from the chlorinated napthalene. It was not possible to establish a hydrochloric acid level, since ferric chloride is also acidic in aqueous solution. These test results indicate that the working fluid was severely decomposed and/or polymerized, leading to the production of ferric chloride, hydrogen, and perhaps HCl.

The O-terphenyl/aluminum (283°) heat pipe has not been sectioned, as further operating time is presently being logged following repair of the heater. Earlier, it was speculated that the O-terphenyl/aluminum reflux capsule was producing hydrogen gas through decomposition of the fluid or an impurity. Unless the oxidized aluminum surface is catalytically decomposing the O-terphenyl, it is unlikely that the fluid itself is the NCG source. The higher temperature pyrolysis data of Figure 2.2-1 can be extrapolated down to 283°C with the result that a gas generation rate less than 1 x (10^{-6}) standard cm^3 per gram per hour would be expected. This would be an insignificant source of NCG over a period of several thousand hours and, hence, the observed gas generation may be attributable to an impurity.

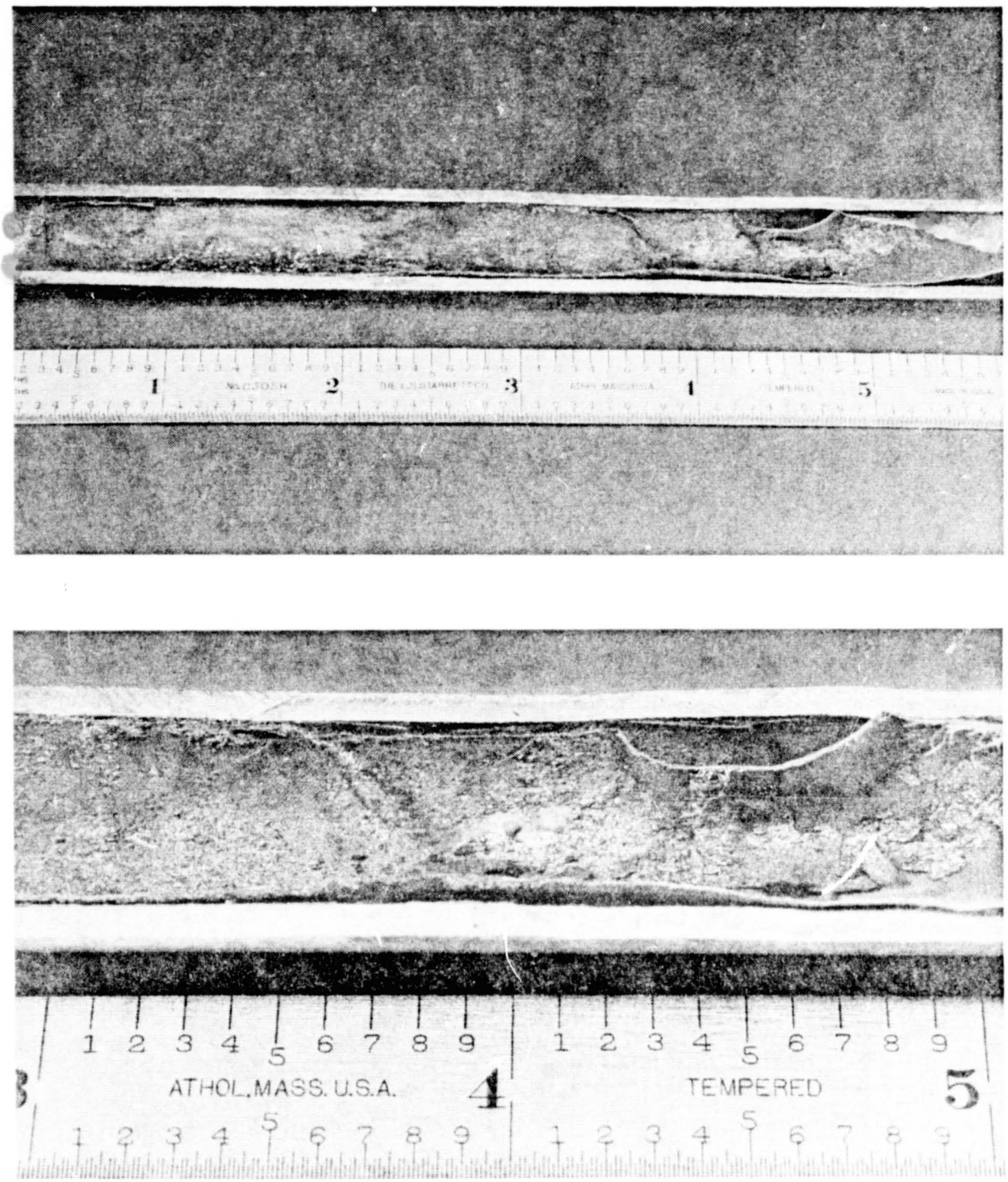

FIGURE 4-4. LONGITUDINAL VIEWS OF MONOCHLORONAPTHALENE/STEEL REFLUX CAPSULE EVAPORATOR AFTER FAILURE AT 266°C. CORROSION OF WICK AND WALL WAS NOT EXTENSIVE, ALTHOUGH CHEMICAL ANALYSES SHOWED IRON AND CHLORIDE IONS IN THE WORKING FLUID. LARGE DEPOSITS OF A BRITTLE DARK AMORPHOUS MATERIAL WERE FOUND, AND THE WORKING FLUID HAD CHANGED FROM A COLORLESS MOBILE LIQUID TO A DARK VISCOUS OIL.

5.0 SUMMARY

This project consisted of a search for stable two-phase heat transfer fluids for the temperature range 100° to 350°C. Because of the large number of potential working fluids, it was necessary to establish the dependence of thermodynamic stability on chemical and structural characteristics, thereby defining classes of compounds with similar chemical and stability behavior. From this ranking, ten fluids were selected for long-term reflux compatibility tests in aluminum and mild steel envelopes. The fluids selected were not necessarily the most stable compounds, but rather represented distinct chemical groups of interest. These groups were

1. Aliphatic hydrocarbons
2. Aromatic hydrocarbons
3. Halogenated hydrocarbons
4. Inorganic molecular fluids

Because of the sensitivity of two-phase heat transfer to noncondensable gases (NCG), the thermal decomposition of working fluids to form NCG was studied in some detail.

Thermal decomposition of a compound can be visualized as a step-wise process of bond breaking, with the weakest bond essentially defining the compound's thermal stability. The constituents of many molecular species are held together with highly localized covalent orbitals called σ bonds, and it is the strength of each σ bond that defines the high-temperature gas phase stability of the compound. Table 2.2-1 is a compilation of organic and halogenated organic bond strengths. Delocalized electronic orbitals found in the aromatic hydrocarbons and other ring structures enhance bond strength, and such compounds generally exhibit superior high-temperature stability. Several aromatic compounds have physical properties (and particularly boiling points) appropriate for the temperature range 100° to 350°C. These include napthalene (218°C), biphenyl (254.9°C), and the o-m-p terphenyls (332-385°C). All can be expected to be rather stable species, and in fact, these materials have been examined as potential reactor coolants. A distinct disadvantage is the relatively high melting points in the range of 50° to 100°C.

Pyrolysis data and bond strength measurements indicate that halogenated straight-chain hydrocarbons are less stable than halogenated ring compounds. In particular, it appears that fluorinated aromatic compounds may present attractive property combinations: The addition of fluorine atoms can greatly alter the melting or boiling points, for example.

In addition to well-known inorganic fluids such as ammonia, water, and sulfur dioxide, there are a large number of inorganic molecular fluids that are of potential interest, particularly metal halides. An inorganic molecular fluid differs from a molten salt in that the liquid phase is composed of molecules rather than ions, and the electrical conductivity is relatively low. Corrosion mechanisms that are accelerated by halide ions in aqueous solution, e.g., stress corrosion, may be inactive in the anhydrous molecular liquid. The inorganic fluids as a group are similar in thermal properties to the organic fluids, and their primary attractions are a potentially higher thermal stability and reduced generation of noncondensable gases. However, some of the fluids are toxic or flammable and must be handled with care. Other potential problems relate to envelope/working fluid chemical reactions. For example, when the working fluid is the halide salt of a metal low on the electromotive series, and the heat pipe envelope is made of a metal high on the electromotive series, there is the possibility that the envelope material will form a halide salt and the less reactive metal will be deposited on the heat pipe wall.

The ten working fluids selected for extended reflux operation included compounds from three of the four fluid categories noted, that is, the aromatic hydrocarbons (toluene, napthalene, biphenyl and O-terphenyl), halogenated aromatic hydrocarbons (monochloronapthalene and 1-fluoronapthalene), and the inorganic molecular fluids (carbon disulphide, tin tetrachloride, titanium tetrachloride, and antimony trichloride). The working fluids were all reagent-grade materials with the exception of monochloronapthalene, which was of undetermined purity. The various fluids have been in test for varying periods of time up to 3500 hours. Each fluid was refluxed within a steel (A-178) and/or an aluminum (type 6061) capsule.

The results of these tests are discussed in Section 4.0, Compatibility Tests. Briefly, of 18 permutations tested, three were found to be totally incompatible at test temperature. These included tin tetrachloride/aluminum operated at 159°C, antimony trichloride/aluminum at 227°C, and monochloronapthalene/steel at 266°C. On the basis of relative chemical activities, these particular inorganic fluids would be expected to be potentially incompatible with the envelopes noted above.

The remaining fluid and envelope combinations generated varying amounts of non-condensable gas, and displayed a variety of differing gas generation kinetics.

6.0 REFERENCES

1. S. Benson, The Foundations of Chemical Kinetics, McGraw-Hill, 1960.
2. K. Ingold, et al., Proc. Roy. Soc. (London), A203, 486, 1950.
3. M. Szwarc, J. Chem. Phys., 16, No. 2, Feb. 1948, p. 128.
4. S. Price, Can. J. Chem., 40, 1962, p. 1310.
5. A. Basiulis, et al., Compatibility and Reliability of Heat Pipe Material 2nd International Heat Pipe Conference, Bologna, Italy, March 31, 1976.
6. S. F. Politanskii and V. U. Shevchuk, Kinet Katal., 1968, 9(3), p. 496.
7. F. Gozzo and C. Patrick, Tetrahedron, 22, 1966, p. 3329.
8. J. Edwards and P. Small, I&EC Fund., 4, No. 4, Nov. 1965, p. 396.
9. J. A. Callighan, ASHRAE J., Sept. 1969, p. 65.
10. F. Norten, Refrigeration Engineering, Sept. 1957, p. 33.
11. E. Steacie and I. Puddington, Can. J. Res., 16, Sec. B, p. 176.
12. E. Steacie and I. Puddington, Can. J. Res., 16, Sec. B, p. 260.
13. S. Benson, The Foundations of Chemical Kinetics, McGraw-Hill, 1960.
14. S. Price, Can. J. Chem., 40, 1962, p. 1310.
15. R. Bolt and J. Carrol, Eds., Radiation Effects on Organic Materials, Academic Press, 1963.
16. Organic Coolant Databook, Tech. Publ. AT-1, Monsanto Chemical Co., July 1958.
17. W. Siefert, L. Jackson, C. Sech, Design and Operational Consideration fo High Temperature Organic Heat Transfer Systems, Process Heat Transfer Symp., 71st Natl AIChE Meeting, Feb. 22-24, 1972, Dallas Texas.
18. G. H. Teletzke, Chemical Engineering Progress, 60 (1), 33-8, 1964.
19. F. J. Norton, Rates of Thermal Decomposition of $CHClF_2$ and CF_2Cl_2, ASHRE 53rd Annual Meeting, Miami Beach, Florida, June 3, 1957.

20. J. A. Callighan, ASHRAE Jour., September, 1969, p. 65.

21. DuPont Product Information Booklet B-33, Thermal Stability of the "Freon" Compounds

22. Dowtherm Heat Transfer Fluids, Dow Chemical Company, 1967.

23. Handbook of Aromatic Fluorine Compounds, Olin Corporation, 120 Long Ridge Road, Stamford, Conn.

24. Brochure Halowax® Chlorinated Napthalene Oils and Waxlike Solids, Koppers Company, Inc., 612 Chatham Center, Pittsburgh, Penn.

25. Personal communication with R. W. Maxwell, Jr., Group Leader, Industrial Chemicals, Koppers Company, Inc., Organic Materials Div., 440 College Park Drive, Monroeville, Penn. 15146.

26. D. R. Miller, et al., Working Fluids for Automotive Rankine Engines, 7th Intersociety Energy Conversion Engineering Conference, San Diego, Cal., 1972.

27. Handbook of Laboratory Safety, Chemical Rubber Company, 1971.

28. N. Sax, Dangerous Properties of Industrial Materials, Van Nostrand Reinhold, New York, 1975.

29. B. R. Sundheim, Fused Salts, McGraw-Hill, New York, 1964.

30. F. Daniels and R. Alberty, Physical Chemistry, John Wiley and Sons, Inc., New York, N.Y., 1963.

31. I.U.K. Delimarskii and B. F. Markov, Electrochemistry of Fused Salts, The Sigma Press, Publishers, 2140 K Street, N.W., Washington, D. C., 1961.

32. G. J. Janz, Molten Salts Handbook, Academic Press, New York, 1967.

33. Handbook of Chemistry and Physics, Chemical Rubber Co., Cleveland, Ohio, 1973.

34. F. Kreith, Principles of Heat Transfer, International Textbook Co., 1967.

35. M. Pourbaix, Atlas of Electrochemical Equilibria in Aqueous Solutions, NACE, Houston, Texas, 1974.

APPENDIX A. FLUID CERTIFICATIONS

TABLE A-1. SPECIFICATIONS FOR HEAT PIPE TEST FLUIDS

Working Fluid (Boiling point, ^{o}C)	Vendor Product Name	Vendor/Number	Specifications
carbon disulphide (46.5^{o})	same	Mallinckrodt 4351	spectrophotometric grade
toluene (110.4^{o})	same	J. T. Baker 1-9460	reagent
tin tetrachloride (114.1^{o})	stannic chloride	MC/B SX875/CB766	anhydrous, purified
titanium tetrachloride (136.4^{o})	same	MC/B TV690/7425	99.5%
1-fluoronapthalene (216^{o})	same	PCR 10047	97-99%, m.p. 9^{o}C, b.p. 215-217^{o}C
napthalene (217.9^{o})	same	J. T. Baker 2718	reagent, m.p. 80-81^{o}C, residue after ignition 0.001
antimony trichloride (219^{o})	same	Mallinckrodt 3624	analytical reagent
monochloronapthalene (250^{o})	chloronated napthalene	Koppers Co. 1031	mixture of isomers
biphenyl (255^{o})	same	J. T. Baker C278	reagent, m.p. 68-70^{o}C
o-terphenyl (332^{o})	same	Eastman 2301	reagent, m.p. 56-58^{o}C